Equilibrium calculations of iron speciation and apparent iron solubility in the Celtic Sea at ambient seawater pH using the NICA-Donnan model

Kechen Zhu[1], Antony J. Birchill[2], Angela Milne[2], Simon Ussher[2], Matthew P. Humphreys[3], Nealy Carr[4], Claire Mahaffey[4], Maeve C. Lohan[5], Eric P. Achterberg[1] and Martha Gledhill*[1]

[1] GEOMAR Helmholtz Center for Ocean Research Kiel, Wischhofstr. 1-3, Kiel, Germany

[2] School of Geography, Earth and Environmental Sciences, University of Plymouth, Plymouth, UK

[3] NIOZ Royal Netherlands Institute for Sea Research, Department of Ocean Systems (OCS), Texel, The Netherlands

[4] School of Environmental Sciences, 4 Brownlow Street, University of Liverpool, L69 3GP, UK

[5] School of Ocean and Earth Science, University of Southampton, Southampton, UK

* Correspondence: mgledhill@geomar.de

Abstract

We used a combined ion pairing - organic matter speciation model (NICA-Donnan) to predict the organic complexation of iron (Fe) at ambient pH and temperature in the Celtic Sea. We optimized our model by direct comparison with Fe speciation determined by Adsorptive Cathodic Stripping Voltammetry using the added Fe-binding ligand 1-nitroso-2-naphthol (HNN) in the presence and absence of natural organic matter. We compared determined Fe speciation with simulated titrations obtained via application of the NICA-Donnan model with four different NICA parameter sets representing a range of binding site strengths and heterogeneities. We tested the assumption that binding sites scale to dissolved organic carbon (DOC) concentrations in marine waters. We found that a constant low DOC concentration resulted in an improved fit of our titration data to the simulated titrations, suggesting that inputs of autochthonous marine DOM may not increase the heterogeneity or concentrations of Fe binding sites. Using the optimal parameter set, we calculated pFe(III)´ (-log($\sum Fe(OH)_i^{3-i}$)) and apparent Fe(III) solubility ($SFe(III)_{app}$) at ambient pH and temperature in the water column of the Celtic Sea. $SFe(III)_{app}$ was defined as the sum of aqueous inorganic Fe(III) species and Fe(III) bound to DOM formed at a free Fe (Fe^{3+}) concentration equal to the limiting solubility of Fe hydroxide ($Fe(OH)_3(s)$). $SFe(III)_{app}$ was within range of the determined dissolved Fe concentrations observed after winter mixing on the shelf and in waters >1500 m depth at our most offshore stations. Our study supports the hypothesis that the ocean dissolved Fe inventory is controlled by the interplay between Fe solubility and Fe binding by organic matter, although the overall number of metal binding sites in the marine environment may not be directly scalable to DOC concentrations.

Keywords: trace metals, ocean acidification, intrinsic binding constants.

Introduction

Iron (Fe) is an essential micronutrient for marine phytoplankton growth, and its low supply and solubility limits primary productivity in large parts of the world's ocean (Boyd and Ellwood, 2010). Iron limitation mostly occurs in high–nitrate, low-chlorophyll (HNLC) regions, which make up approximately 30% of the surface ocean (Boyd et al., 2007). However, both Fe limitation and the potential for seasonal Fe limitation have also been reported for coastal regions and shelf seas, including European shelf seas (Birchill et al., 2017; Hogle et al., 2018; Hutchins & Bruland, 1998). The bioavailability and solubility of Fe in seawater is a function of its chemical speciation (Boyd & Ellwood, 2010; Gledhill & Buck, 2012; Hutchins et al., 1999). Inorganic Fe(III) is the thermodynamically favoured form of Fe in oxygenated seawater but, as a result of hydrolysis (equation 1), it has a low solubility that reaches a minimum between pH 7 and 9 (Byrne et al., 2000; Kuma et al., 1996; Liu & Millero, 2002). Hydrolysis competes with binding by organic matter (equation 2), thus complexation by dissolved organic ligands (i.e. those <0.2 μm in size) has the potential to reduce free Fe^{3+} concentrations and consequent formation of insoluble iron hydroxides ($Fe(OH)_3(s)$) and thereby increase the concentration of Fe(III) observed in the dissolved fraction (<0.2 μm) (Kuma et al., 2000, 1996; Liu and Millero, 2002).

$$Fe^{3+} + 3OH^- \rightarrow Fe(OH)_3(s) \quad (1)$$

$$2Fe^{3+} + (3-i)OH^- + DOM^{x-} \leftrightarrow Fe(OH)_i^{3-i} + Fe(DOM)^{3-x} \quad (2)$$

Reduction to Fe(II), via e.g. photolysis or biological activity, can also change Fe speciation, potentially increasing both the bioavailability and solubility of Fe (Barbeau, 2006; Rose and Waite, 2005; Schlosser et al., 2018). Complexation by organic matter, hydrolysis, and redox speciation thus all play important roles in ocean Fe biogeochemistry, and as a result the global Fe cycle is influenced by ocean acidification, water column stratification, warming and deoxygenation (Hutchins & Boyd, 2016). Given the role of Fe as an essential micronutrient, there is thus a need to develop reliable approaches that can be used to predict the impact of environmental change on oceanic Fe speciation and biogeochemistry (Ye et al., 2020). Ideally, such approaches would be based on a set of intrinsic (i.e. independent of the physico-chemical characteristics of the water sample such as temperature, pH and ionic strength) thermodynamic and kinetic constants that would describe the chemical speciation

and rates of reaction of all Fe species in seawater according to ambient temperature, salinity and pH (Turner et al., 2016; Ye et al., 2020).

With respect to Fe(III) speciation in seawater, the work of Liu and Millero (1999) and Byrne et al. (2000) has provided a set of intrinsic thermodynamic constants that describe Fe hydrolysis and the formation of fresh Fe(III)-hydroxide colloidal precipitates (retained on a 0.02 µm filter). In contrast, for organic complexation, determination of metal speciation in seawater has traditionally adopted an approach where the observed strength and concentrations of metal-binding ligands were related to specific conditions of the sample (i.e. salinity, dissolved Fe concentration) and analysis (i.e. pH typically 8.0-8.2 depending on the method employed). Ocean sections of conditional ligand concentrations published as part of the GEOTRACES research programme (Buck et al., 2018, 2015; Gerringa et al., 2015) showed that, at pH 8 and room temperature, average conditional ligand concentrations range from 1-2 equivalents of Fe binding sites (nmol L^{-1}), and typically correlate with dissolved Fe concentrations, exceeding them by an average of ca.1 equivalents of Fe binding sites (nmol L^{-1}) (Caprara et al., 2016). This covariance can at least partially be explained by application of analytical experimental designs and mathematical transformations that simplify a heterogeneous group of binding sites to an "average" site that can be observed under the applied experimental conditions (for further information see e.g. Gledhill and Buck, (2017); Town and van Leeuwen, (2005)). Thus, whilst the conditional approach demonstrates that organic complexation is important for the biogeochemistry of Fe, the conditional nature of the obtained results constrains our ability to predict how Fe(III) speciation is likely to change in a future ocean, since it provides no mechanistic knowledge of how Fe(III) binding to organic matter is influenced by pH or temperature.

Exactly how Fe(III) binding to organic matter changes as a function of pH depends on the functional group characteristics of the metal binding components of marine dissolved organic matter (DOM) (Shi et al., 2010; Zhang et al., 2019). Dissolved organic matter is a highly diverse mix of compounds (Koch et al., 2008) that will also potentially change in a future ocean (Lønborg et al., 2020). Metal binding components likely make up only a minor subset of the overall DOM pool (Zhang et al., 2019). Previous studies have shown that bacteria and phytoplankton can release Fe binding ligands, including siderophores and polysaccharide exudates into their environment (Hassler et al., 2011a; Hassler et al., 2011b; Mawji et al., 2011; Vraspir and Butler, 2009). In addition, ligands can be released following viral lysis (Poorvin et al., 2011) or delivered by terrigenous sources in the form of

127 humic-like substances (Laglera et al., 2019; Muller, 2018). Terrigenous DOM has furthermore been
128 shown to dominate Fe binding in certain oceanic regions like the Arctic Ocean (Laglera et al., 2019;
129 Slagter et al., 2019; Sukekava et al., 2018). The organic ligand pool thus shows an intrinsic chemical
130 heterogeneity, which is still not well understood (Gledhill and Buck, 2012), but is likely analogous to
131 metal binding to natural organic matter in terrestrial and freshwater environments (Lodeiro et al.,
132 2020).
133
134 Binding models for describing metal binding to organic matter using intrinsic constants that account
135 for heterogeneity are widely applied in terrestrial and freshwater environments. Perhaps the most
136 widely used models are the Non-Ideal Competitive Adsorption (NICA)-Donnan model (Kinniburgh
137 et al., 1999), Windermere humic acid model (WHAM) (Tipping et al., 2011), and Stockholm humic
138 model (SHM) (Gustafsson, 2001). A primary assumption in these models is that binding sites scale
139 proportionally to the concentration of dissolved organic carbon (DOC; 'dissolved' in this context is
140 typically defined as <0.7 μm in size). The appeal of such an approach lies in the potential for
141 describing the influence of Fe(III) binding to organic matter as a function of ambient pH and DOC
142 concentrations, using a limited set of constants that could be applied to the estimation of Fe
143 speciation across the whole ocean (Hiemstra and van Riemsdijk, 2006; Stockdale et al., 2016).
144 Indeed, a step in this direction has recently been made in Ye et al. (2020), where the NICA-Donnan
145 model has been used to parameterise the impact of future changes in ocean pH on ocean productivity
146 in a global biogeochemical model. The NICA-Donnan model describes the binding behavior of metal
147 ions to a heterogeneous mix of binding sites using a continuous bimodal distribution based on the
148 Langmuir-Freundlich adsorption isotherm (Kinniburgh et al., 1999), while both the WHAM and
149 SHM models rely on a set of empirically derived relationships and a set number of binding sites with
150 different affinities to calculate metal speciation (Gustafsson, 2001; Tipping et al., 2011). A further
151 key difference between the three approaches relates to the application of electrostatic sub-models to
152 describe the impact of ionic strength on binding of metals to the organic matter phase. In the NICA-
153 Donnan model, the Donnan component is used to describe non-specific electrostatic interactions on
154 metal binding to DOM, while the SHM model uses the Basic Stern model (Gustafsson, 2001) and
155 WHAM uses a correction based on the Debye-Hückel and Gouy-Chapman theory (Tipping et al.,
156 2011). All three approaches have been successfully used to predict metal speciation in seawater
157 (Avendaño et al., 2016; Hiemstra & van Riemsdijk, 2006; Ndungu, 2012; Stockdale et al., 2011,

158 2015; Tipping et al., 2016). However, since a direct intercomparison study has yet to be undertaken,
159 it is not known if one model is superior to the others in seawater applications.
160
161 In order to further test the applicability of such heterogeneous models to Fe(III) speciation in the
162 marine environment, we wished to examine predicted and observed relationships between DOC
163 concentrations and Fe speciation in more detail. In this study, we tested the underlying assumption
164 that Fe speciation determined with a given set of intrinsic NICA constants could be scaled to DOC
165 concentrations, at least within the range of DOC concentrations typically observed in marine waters.
166 In coastal waters, average DOC concentrations are ca. 300 µmol L^{-1} because of enhanced
167 productivity or localized DOC inputs from terrestrial sources (Barrón and Duarte, 2015), while in the
168 open ocean DOC concentrations are lower and vary by at most a factor of two (40-80 µmol L^{-1},
169 Hansell, 2013). Since DOM composition changes with DOC concentration (Hansell, 2013), we also
170 implicitly tested a second assumption, that the changes in DOM composition resulting from
171 microbial production and utilization of organic matter does not significantly impact the binding
172 properties of DOM when expressed relative to DOC concentrations. We used samples collected on
173 three cruises in the Celtic Sea during three different seasons. The Celtic Sea is a productive,
174 temperate sea located on the northwest European shelf (Carr et al., 2018; Muller-Karger et al., 2005).
175 Our three cruises transected from a productive shelf environment out to the open ocean and our
176 samples therefore incorporated a range of DOC concentrations and DOM compositions from
177 autochthonous marine DOM produced during phytoplankton bloom conditions to aged DOM from
178 deep waters (>500 m). We compared the concentrations of observed Fe species to those predicted
179 using four sets of NICA constants representative of different degrees of heterogeneity and overall
180 binding strength. Two sets of NICA constants were previously described in the literature (Gledhill et
181 al., 2015; Hiemstra and van Riemsdijk, 2006) and two sets were re-derived from raw titration data
182 obtained in a previous study in our region (Avendaño et al., 2016) and were thus more specific to
183 DOM in our research area. We used the NICA-Donnan model to calculate the equilibrium speciation
184 of Fe(III) at ambient pH and temperature in our region. We estimated the impact of Fe bound to
185 organic matter on the inorganic Fe fraction (Fe´) in our study region. Since Fe(III) solubility is also
186 directly related to Fe speciation, we also examined the saturation state of Fe^{3+} with respect to
187 $Fe(OH)_3(s)$ at ambient pH and temperature in our study region by calculating the apparent Fe(III)
188 solubility ($SFe(III)_{app}$). We define $SFe(III)_{app}$ as the sum of aqueous inorganic Fe(III) species and
189 Fe(III) bound to DOM formed at a free Fe (Fe^{3+}) concentration equal to the limiting solubility of Fe

hydroxide ($Fe(OH)_3(s)$; Zhu et al., 2021). We discuss the observed trends in the context of observed total dissolved Fe concentrations in order to understand the relative importance of different physico-chemical drivers that influence Fe speciation.

Materials and Methods

Sampling

Samples were collected during three cruises: DY018 in autumn (November 2014), DY029 in spring (April 2015) and DY033 in summer (July 2015) in the Celtic Sea on board the RRS Discovery as part of the UK Shelf Sea Biogeochemistry programme (Birchill et al., 2017; Rusiecka et al., 2018). Here, we examine Fe speciation at the central Celtic Sea site (CCS), a shelf edge station (CS2) and an off-shelf transect through a submarine canyon (C01-06) (Figure 1). Salinity, depth and temperature were measured using a Seabird CTD attached to a titanium rosette frame equipped with 24 x 10 L Ocean Test Equipment bottles (Birchill et al., 2017). Trace metal samples were collected following GEOTRACES protocols (Cutter et al., 2017). Samples for the determination of Fe speciation were filtered (0.2 µm cartridge filters; Sartobran-300, Sartorius) into acid-cleaned 250 ml low density polyethylene (LDPE) bottles (Nalgene) and frozen immediately (-20 °C). Samples were subsequently analyzed in a trace metal clean laboratory at GEOMAR.

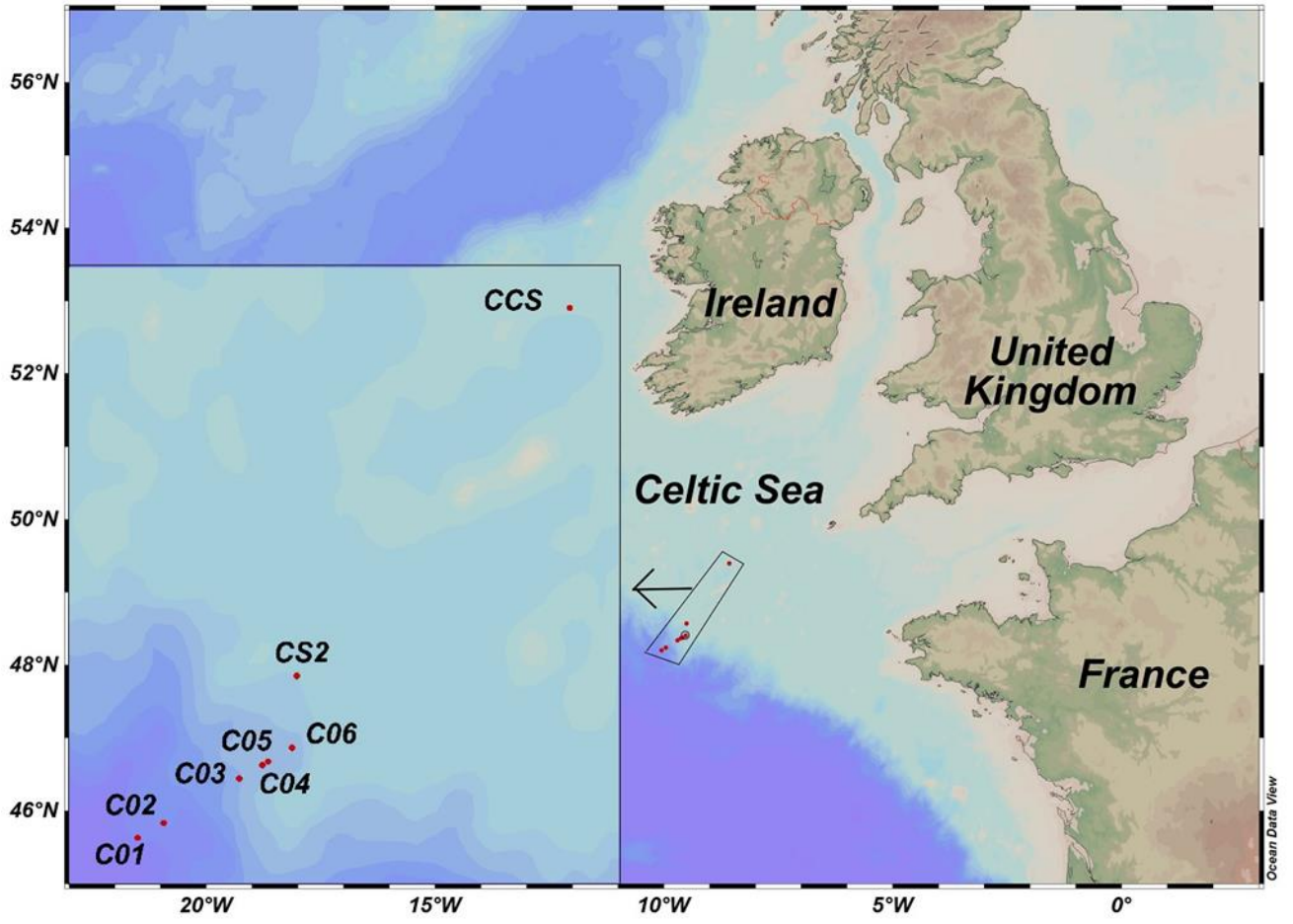

Figure 1. Map of study area with stations indicated by red dots. Map generated using Ocean Data View (Schlitzer, 2015).

Determination of dissolved Fe, dissolved organic carbon and pH

Samples for DFe analysis were collected after filtration through 0.2 µm cartridge filters. The samples were stored in acid cleaned LDPE bottles (Nalgene) and acidified to pH 1.7 (0.024 mol L^{-1} HCl, Romil-UpA). Dissolved Fe concentrations were determined using flow injection with chemiluminescence detection (Birchill et al., 2017; Obata et al., 1993). The accuracy and analytical uncertainty of the method was assessed by applying the top down NordtestTM approach to the analysis of SAFe and GEOTRACES consensus materials, the combined uncertainty was calculated to be 9.5 % (Worsfold et al., 2019).

Samples for the determination of DOC were collected after filtration (ashed glass fibre filters, 0.7 µm nominal pore size, Whatman), and acidified to pH 2 using hydrochloric acid. The DOC samples were analyzed onshore using high temperature catalytic oxidation on a Shimadzu TOC-VCPN. Consensus

reference materials (CRM; University of Miami) were used to determine accuracy and precision of analysis daily, which were both better than 4 %.

Samples for dissolved inorganic carbon (C_T) and total alkalinity (A_T) were collected via silicone tubing into 250 ml borosilicate glass bottles following established protocols (Dickson, 2010). For the off-shelf transect, samples for C_T and A_T were collected only during DY018 and DY033. Each bottle was sealed shut with a greased ground glass stopper after introducing a 2.5 ml air headspace and sterilising the sample with 50 µl of saturated mercuric chloride solution. All samples were stored in the dark until analysis with VINDTA 3C instruments (Marianda, Germany). The C_T and A_T measurements were calibrated using measurements of certified reference material obtained from Prof A. G. Dickson (Scripps Institution of Oceanography, USA) (Humphreys et al., 2019). The pH of our seawater samples was calculated on the IUPAC/NBS scale (pH_{NBS}) from C_T and A_T using CO2SYS (Pierrot et al., 2006). In CO2SYS, the constants describing the carbonate and sulphate equilibrium with hydrogen ions were from Mehrbach et al. (1973) (refitted by Dickson and Millero (1987)) and Dickson, (1990), respectively, and the total boron concentration was estimated from salinity following Uppström, (1974). We used the NBS pH scale because it is consistent with the speciation constants in the applied NICA-Donnan and ion pairing models.

Determination of iron speciation via adsorptive cathodic stripping voltammetry

Iron speciation was determined by competitive ligand equilibrium with adsorptive cathodic stripping voltammetry (CLE-AdCSV), using 1-nitroso-2-naphthol (HNN) as the added ligand (van den Berg, 1995). HNN (Sigma-Aldrich) was diluted in methanol (Fisher, HPLC grade) to make a stock solution. To clean the stock buffer solution of N-(2-Hydroxyethyl)piperazine-N′-(2-ethanesulfonic acid) (HEPES; Sigma-Aldrich), HNN was added and equilibrated with the buffer overnight. HNN and $FeNN_3$ were subsequently removed using a pre-activated C18 SepPak column (Whatman). The pH_{NBS} of the buffer solution was adjusted to 8 prior to the titration work with ammonium hydroxide (20-22%) (Optimal, Fisher Scientific), and the pH_{NBS} of each buffered sample was determined to be between 7.9 and 8.1, with an overall average of 8.00±0.08 (n=93).

Since the speciation measurements are thermodynamic, it is important that voltammetric peaks are stable and equilibrium is achieved (Laglera & Filella, 2015; Van Leeuwen & Town, 2005). In previous studies, a reaction time of > 6 h was assumed to be sufficient to reach equilibrium

conditions (Avendaño et al., 2016; Boye et al., 2001; Boye et al., 2003; Gledhill & van den Berg, 1994). However, Wu and Luther (1994, 1995) waited 24 h to reach the equilibrium condition between FeL (i.e. Fe bound to natural ligand) and HNN. Here, we tested equilibration time prior to analyzing Fe speciation in our seawater samples. Our test indicated that a reaction time > 12h was needed to obtain consistent, reproducible peak heights, which we took to approximate equilibrium conditions between FeL and HNN for our method and we therefore allowed for a 16 h equilibration period.

Our speciation measurements are based on establishing an equilibrium between HNN, Fe^{3+}, binding sites (L^-) and the remaining inorganic Fe species (e.g. hydroxides) in the solution. The ratio of free to complexed species gives the side reaction coefficient (α) for the reaction (Ringbom and Still, 1972), which is also related to the conditional stability constant ($k^{cond}_{FeNN3,Fe3+}$) and the concentration of ligand not bound to Fe ([NN´]), as shown for the formation of $FeNN_3$ in equation (3).

$$\frac{[FeNN_3]}{[Fe^{3+}]} = \alpha'_{FeNN3,Fe3+} = k^{cond}_{FeNN3,Fe3+} \times [NN']^3 \quad (3)$$

Species can only compete when their side-reaction coefficients are within an order of magnitude of each other, hence ligands detectable in a CLE-AdCSV titration are restricted to those with side reaction coefficients (α'_{FeL}) within this "detection window" (Apte et al., 1988; Hudson et al., 2003; Nimmo et al., 1989; Voelker and Kogut, 2001). However, there may be a considerable range of ligand strengths in seawater and the use of at least two detection windows has previously been recommended to ensure the full range of ligand strengths can be accounted for (Buck et al., 2012; Pižeta et al., 2015; Sander et al., 2011). We therefore used three different total HNN concentrations, $[HNN_T]$ = 1, 5 and 20 µmol L^{-1}.

We combined our different HNN concentrations with seven different Fe additions between 0 and 5 nmol L^{-1} at the two lower HNN concentrations (1 and 5 µmol L^{-1}) and 3 concentrations (5, 10, 15 nmol L^{-1}) at the highest HNN concentration (20 µmol L^{-1}) to create a matrix of 18 titration points. All titration data for one sample were obtained on the same day. Our aim was to estimate the slope using our highest HNN concentration and calculate $[FeNN_3]$ according to the "overload titration" method (Kogut and Voelker, 2001). Examination of the sensitivity observed for each HNN concentration in seawater in our samples at Fe concentrations ≥ 3 nmol L^{-1} showed no significant difference between

sensitivity at 5 and 20 µmol L^{-1} HNN (details in supplementary information, Figure S1). On the other hand, the titration point with the highest added Fe concentration (15 nmol L^{-1}) was often lower than expected, suggesting non-linearity in the titration at higher Fe concentrations, possibly caused by adsorption of the hydrophobic $FeNN_3$ complex on the walls of the voltammetric cell (Supplementary Figure S2). We thus used the data with 5 and 20 µmol L^{-1} HNN and added Fe concentrations from 3 to 10 nmol L^{-1} to calculate the sensitivity of our analysis and determine the $FeNN_3$ concentration.

The concentration of HNN not complexed by Fe ([NN´]) and the conditional stability constant ($k^{cond}_{FeNN3,Fe3+}$) of the $FeNN_3$ complex were used to derive the free Fe^{3+} concentrations in the sample at the fixed titration pH_{NBS} of 8.0 over the range of Fe concentrations according to equation (3). Since $[HNN_T] >> [Fe]$, we assumed that $[HNN_T] = [NN´]$. The cumulative random error for Fe^{3+} is largely dependent on the random error in the $FeNN_3$ concentration, as the 95 % confidence interval for the estimation of $k^{cond}_{FeNN3,Fe3+}$ was 0.2 % of the determined value (see results). We estimated an average analytical precision for our determined $FeNN_3$ concentrations of 9 % based on the mean variability of observed peak areas. However, we note this estimate does not account for errors incurred during calculation of the sensitivity, which will result in an additional random error between titrations, or the potential increase in error that is likely to occur as peak heights decrease.

The difference between the total Fe present in the solution and $[FeNN_3]$ were used to determine the non-labile dissolved Fe concentration (DFe*):

$$DFe^* = [TFe] - [FeNN_3] \quad (4)$$

where [TFe] is the concentration of total Fe (i.e. DFe + added Fe). DFe* is subject to error propagation from the determinations of both $FeNN_3$ (9 %) and dissolved Fe (7 %) and thus will be subject to the combined error of 11.4 %. We therefore only report values of DFe* where $[FeNN_3]$ is at least 11.4 % less than [TFe].

<u>Derivation of equilibrium constant for $FeNN_3$ for application in ion pairing models for seawater</u>

To ensure consistency between our observed $FeNN_3$ concentrations and our speciation calculations we derived an equilibrium constant valid for seawater (S=35) between pH_{NBS} 7.2-8.5 that accounts for competition between Fe and hydrogen ions for NN^-.

$$Fe^{3+} + 3HNN \leftrightarrow FeNN_3 + 3H^+ \quad (5)$$

We distinguish this constant from previously derived conditional stability constants ($\log k^{cond}_{FeNN3,Fe3+}$) by denoting it $\log k_{FeNN3,H+}$. We used the equilibrium constant for HNN of $10^{7.9}$ (NIST, Smith et al. 2004). Derivation was carried out by combining the chemical speciation program ORCHESTRA (Meeussen, 2003) with the parameter estimation software PEST (Doherty, 2019). Speciation calculations in ORCHESTRA were set up with input, chemistry and objects files as described previously (Janot et al., 2017; Zhu et al., 2021). Further details can be downloaded from protocols.io (dx.doi.org/10.17504/protocols.io.brc4m2yw). We used the Minteqv4 database for thermodynamic constants, which is consistent with the database used previously in visual MINTEQ (Avendaño et al., 2016; Gledhill et al., 2015) and we also verified that calculations in ORCHESTRA and visual MINTEQ were comparable. For the derivation of $\log k_{FeNN3,H+}$ we specified an initial estimate of 31 (Avendaño et al., 2016; Gledhill et al., 2015), with an allowed range of 28 to 32. Parameter derivation is performed by calculation of the $FeNN_3$ concentration in ORCHESTRA for each measurement, which is then passed to PEST and compared to the observed values. PEST provides a new value for $\log k_{FeNN3,H+}$, which is then passed back to ORCHESTRA for a fresh calculation of $FeNN_3$. The procedure is iterated to minimize the residuals between observed and calculated $FeNN_3$ calculations via the Levenberg-Marquardt algorithm. The PEST output comprises a value for $\log k_{FeNN3,H+}$ with 95% confidence intervals, together with a full record of the optimization in the output file. Consistency was then further assessed by comparison between observed and calculated $FeNN_3$ and Fe^{3+} in UV irradiated seawater as a function of HNN concentration, within the HNN concentration range applied in this study.

Assessment of relationship between observed and calculated concentrations of iron species to DOC concentrations assuming binding sites behave according to the NICA-Donnan model.

The NICA-Donnan model was used to calculate the speciation of Fe at equilibrium for each titration point at pH_{NBS} 8.0, via speciation calculation tool ORCHESTRA (Meeussen, 2003). We tested the assumption that one set of NICA-Donnan parameters could describe variability in [$FeNN_3$] and [Fe^{3+}] by adding the "Fulvic acid" NICA-Donnan adsorption model to the dissolved ion pairing model used for the derivation of $\log k_{FeNN3,H+}$. Marine DOM was thus considered analogous to terrestrial and freshwater DOM (Gledhill et al., 2015; Laglera & Van Den Berg, 2009; Lodeiro et al., 2020). The

applied NICA model assumes a continuous Sips bimodal distribution of binding sites. The distribution of the affinities of the two groups of binding sites (Denoted (1): Carboxylic-type groups, and (2): Phenolic-type groups) are described by three constants per binding site group: the width of the binding site distribution (p_1 and p_2), NICA affinity constant ($\log K_{Me1}$ and $\log K_{Me2}$ for a metal cation or $\log K_{H1}$ and $\log K_{H2}$ for the protonation constants) which represents the median of the distribution, and non-ideality constant which represents non-ideal behavior of ion adsorption (n_{Me1}, n_{Me2}, n_{H1}, n_{H2}), where n_{Hi} is <1 (Kinniburgh et al., 1999). The binding of a metal by marine DOM, Q_{Me} is then described with reference to proton binding by marine DOM according to the following equation:

$$Q_{Me} = Q_{max1,T}\frac{n_{Me,1}}{n_{H1}}\cdot\frac{(K_{Me,1}.C_{Me})^{n_{Me,1}}}{(K_{H,1}.C_H)^{n_{H,1}}+(K_{Me,1}.C_{Me})^{n_{Me,1}}}\cdot\frac{\{(K_{H,1}.C_H)^{n_{H,1}}+(K_{Me,1}.C_{Me})^{n_{Me,1}}\}^{p_1}}{1+\{(K_{H,1}.C_H)^{n_{H,1}}+(K_{Me,1}.C_{Me})^{n_{Me,1}}\}^{p_1}}+$$
$$Q_{max2,T}\frac{n_{Me,2}}{n_{H2}}\cdot\frac{(K_{Me,2}.C_{Me})^{n_{Me,2}}}{(K_{H,2}.C_H)^{n_{H,2}}+(K_{Me,2}.C_{Me})^{n_{Me,2}}}\cdot\frac{\{(K_{H,2}.C_H)^{n_{H,2}}+(K_{Me,2}.C_{Me})^{n_{Me,2}}\}^{p_2}}{1+\{(K_{H,2}.C_H)^{n_{H,2}}+(K_{Me,2}.C_{Me})^{n_{Me,2}}\}^{p_2}} \quad (6)$$

where $Q_{max1,T}$, $Q_{max2,T}$ refer to the total number of proton binding sites per binding site type, and C_H and C_{Me} are the concentrations of protons and metal, respectively.

In the NICA-Donnan model, electrostatic interactions are described by the Donnan component of the model which is based on the Boltzmann equation (Benedetti et al., 1996). However, at the ionic strength of seawater the apparent Donnan volume becomes very small and concentrations of metals electrostatically associated with DOM become negligible (Lodeiro et al., 2020; Pinheiro et al., 2021).

In this study, we used two previously published sets of NICA constants and two new NICA parameter sets (Table 1). The previously published sets were derived from surface waters collected in the Sargasso Sea (Set A: Hiemstra and van Riemsdijk, 2006) and surface waters obtained from an estuarine system on the English south coast (Set B: Gledhill et al. 2015), whilst the new parameter set C was re-derived from surface waters in the Northwest European Shelf Sea based on titration data obtained in Celtic Sea samples first reported in Avendaño et al. (2016). We re-derived the set C values because the original reported values were empirically estimated using a $\log k_{FeNN3,H+}$ of 32.5, which was considerably higher than the value we derived in this study (see results). We further examined the impact of n_i by increasing the value of n_1 and n_2 (set D) to consider the possibility that marine DOM is less heterogeneous than typically observed for terrestrial organic matter (Lodeiro et

al., 2020; Zhu et al., 2021). We used PEST-ORCHESTRA to re-derive the NICA constants following a similar procedure used for the derivation of $\log k_{FeNN3,H+}$ and described in Zhu et al., (2021). Since this work was focused on the Celtic Sea, we only used the titration data obtained from Celtic Sea samples in this derivation (samples collected at stations 1, 3, 4, 5, 6 18, 19, 20 from Avendaño et al. (2016)). We provide the raw titration data, required input files and a description of the protocol used in this derivation on protocols.io (dx.doi.org/10.17504/protocols.io.brc4m2yw). We followed the PEST-ORCHESTRA approach that was first used to derive NICA constants for Cd and Zn binding to Laurentian fulvic acid by Janot et al. (2017). Typically, both equilibrium constants and non-ideality constants are derived from experimental data. However, we found during preliminary derivations that since titrations were undertaken at only three pH_{NBS} values (7.2, 7.6, 8) and encompassed a relatively narrow pH range, data from Avendaño et al. (2016) were not sufficiently well constrained in pH space to reproducibly derive all four parameters. We therefore fixed $n_{Fe(III)1}$ and used the relationship between n_1 and n_2 from Milne et al. (2003) ($n_2 = 0.76 \times n_1$) to calculate $n_{Fe(III)2}$. We then estimated $\log K_{Fe(III)1}$, $\log K_{Fe(III)2}$ using initial estimates of 3 and 9, and allowed ranges of 2 to 4 and 8 to 10, respectively. Generic parameters from Milne et al. (2003), (2001) were used to describe binding of proton and major cations (H^+, Ca^{2+}, Mg^{2+}, Sr^{2+}) to be consistent with parameter sets A and B.

To investigate goodness of fit at different ambient DOC concentrations, we compared our observed $FeNN_3$ concentrations with $FeNN_3$ concentrations calculated in ORCHESTRA. We then compared Fe^{3+} calculated from observations using equation (3) with those calculated in ORCHESTRA and observed versus calculated DFe* calculated using equation (4). For speciation calculations, pH was set to the analysis pH_{NBS} (= 8.00±0.08).

Prediction of apparent Fe(III) solubility and inorganic Fe concentrations at ambient pH and temperature in our study region

We predicted Fe speciation in our study area at ambient pH and temperature using the NICA constants with the best fit to our observed titration data. To calculate $SFe(III)_{app}$ we set our total Fe(III) concentration to 10 nmol L^{-1} and allowed for the formation of $Fe(OH)_3(s)$ (ferrihydrite) within ORCHESTRA. We use a solubility product of $\log^* K_s = 3.2$, derived from (Liu and Millero, 1999) to determine iron solubility according to equation (7).

$$^{*}K_S = [Fe^{3+}] \div [H^+]^3 = 10^{3.2}, \Delta H_r = -100.4 \text{ kJ mol}^{-1} \quad (7)$$

We therefore consider organically bound Fe as soluble, but $Fe(OH)_3(s)$ as insoluble. We compare our $SFe(III)_{app}$ with observed dissolved Fe concentrations. However, given the potential size of both freshly formed $Fe(OH)_3(s)$ (defined in Liu and Millero (1999) as >0.02 µm) and organic matter (determined in the < 0.7 µm fraction), the Fe associated with both DOM and $Fe(OH)_3(s)$ may both be colloidal in nature (>0.02 but <0.2 µm) and this should be kept in mind when comparing the absolute values.

We calculated the sum of soluble inorganic species and express these concentrations as pFe(III)´ using:

$$pFe(III)' = -Log\ ([FeOH^{2+}] + [Fe(OH)_2^+] + [Fe(OH)_3] + [Fe(OH)_4^-]) \quad (8)$$

In these calculations, we set the total Fe concentration to be equal to the determined DFe concentration, but $Fe(OH)_3(s)$ was also allowed to form to account for possible formation of insoluble iron hydroxides when Fe^{3+} becomes oversaturated, according to equation (7).

Results and Discussion

<u>Establishing consistency between observations and calculations in the absence of organic matter.</u>

An understanding of how pH and temperature might influence trace element speciation at equilibrium can be obtained via iterative algorithms based on thermodynamic principles using sets of thermodynamic constants valid for the physico-chemical conditions to be explored in the study. We applied "off the shelf" ion pairing software packages in our study that incorporate ionic strength corrections based on the extended Debye-Hückel equation, but we highlight this is not fully optimal and warn that absolute values predicted via our speciation calculations will be affected by systematic bias as a result of overestimation of activities. The impact of the ion pairing approach is illustrated by an approximate 15% underestimation in ionic strength in our calculation (I=0.6 M compared to I=0.7 M typically assumed for seawater), which is consistent with previous estimates of the error introduced by application of the Debye-Hückel equation (Stockdale et al., 2016). Nevertheless, valuable information – with respect to the extent that changes in physico-chemical properties such as

pH and temperature may have on metal speciation – can be obtained if a system can be calibrated such that its observed and calculated values are consistent for a given critical species. In our study, we used a value for $\log k_{FeNN3,H+}$ within an ion pairing model, which would account for competition between NN^-, H^+, Fe^{3+} and OH^- at the ionic strengths and pH relevant to our study. In previous work, a first attempt at such a system was made by manually changing constants to obtain an empirical estimate for $\log k_{FeNN3,H+}$ (Avendaño et al., 2016). In this study, we sought to improve on this by first calibrating $\log k_{FeNN3,H+}$. We particularly focused on establishing consistency between determined and calculated Fe^{3+} and $FeNN_3$ concentrations, since $FeNN_3$ is the measured species from titrations and Fe^{3+} is the Fe species that reacts with the added ligand, hydroxide ion and natural organic matter.

Estimation of $\log k_{FeNN3,H+}$ using the parameter estimation software package PEST (Doherty, 2019) in combination with the ion pair speciation program ORCHESTRA (Meeussen, 2003) resulted in a $\log k_{FeNN3,H+}$ of 29.5±0.1. With this value, the Pearson correlation coefficient between observed and calculated log[$FeNN_3$] was 0.962 with a root mean squared error (RMSE) of 1.12 nmol L^{-1} over the pH_{NBS} range 7.2-8.5 and at an HNN concentration of 2 µmol L^{-1}. Predicted Fe^{3+} concentrations (Fe^{3+}_{calc}) correlated with Fe^{3+} calculated from the observed $FeNN_3$ concentrations ($Fe^{3+}_{titration}$) ($\log[Fe^{3+}]_{calc} = 0.95 \times \log[Fe^{3+}]_{titration} - 0.83$, $r^2 = 0.97$, n=456) (Figure 2a). The modelled distribution of the relative proportion of Fe present as $FeNN_3$ as a function of pH suggests that $FeNN_3$ will be the dominant species between pH_{NBS} 7 and 8, with a maximum predicted response at pH_{NBS} 7.5 (Figure 2b), which is consistent with the relationship between pH and the voltammetric response for $FeNN_3$ previously reported by van den Berg (1991). However, our derived value of 29.5 for $\log k_{FeNN3,H+}$ is three orders of magnitude lower than the empirical estimate of 32.5 given by Avendaño et al. (2016). Further comparison with literature values showed that our calculated conditional stability constant at pH_{NBS} 8 is within the reported range after calibration against hydroxide and EDTA but lower than obtained at pH_{NBS} 6.9 (Supplementary Table 1). The difference between the calibrated constants could be explained by the ionic strength corrections applied during the calculations, the choice of conditional constants for Fe binding to EDTA, and the applied inorganic side reaction coefficient for Fe (Laglera et al., 2011).

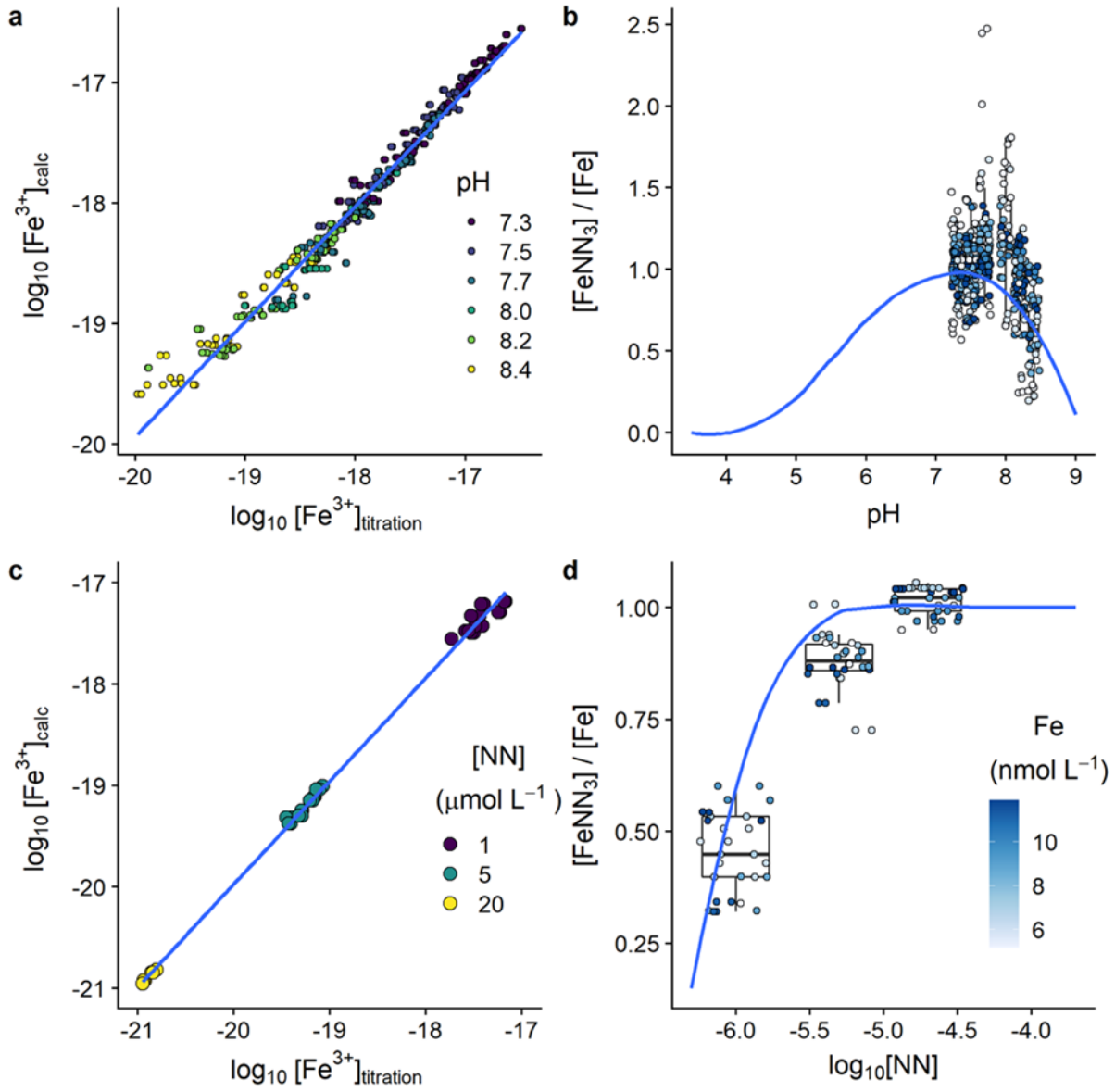

Figure 2 Predicted Fe^{3+} and $FeNN_3$ for seawater after ultra violet irradiation to destroy organic matter. (a) Predicted Fe^{3+} is plotted versus determined Fe^{3+} from titrations using HNN concentrations at 2 and 5 µmol L^{-1} over the pH_{NBS} range 7.2-8.5 (number of observations, n = 456). (b) The proportion of $FeNN_3$ relative to total Fe from titrations using HNN concentrations at 2 and 5 µmol L^{-1} is shown over the pH_{NBS} range 7.2-8.5, where measured $FeNN_3$ is indicated as colored points and predicted $FeNN_3$ is shown by the solid line. The colours represent different Fe concentrations (see legend in d) and n = 456 (c) Predicted Fe^{3+} is plotted versus determined Fe^{3+} from titrations undertaken at constant pH_{NBS} (~8.0) over the range of HNN concentrations. The line shows the 1:1 relationship (n=98). (d) The proportion of $FeNN_3$ relative to total Fe from titrations undertaken at constant pH_{NBS} (~8.0), is shown over the range of HNN concentrations, where measured $FeNN_3$ concentrations are shown as colored points and predicted $FeNN_3$ is shown by the solid line (n=98).

We next examined the relationship between calculated and determined $FeNN_3$ and Fe^{3+} concentrations using the derived $\log k_{FeNN3,H+}$ over the range of HNN concentrations (1, 5 and 20

μmol L^{-1}) employed in this study at pH_{NBS} 8.0 using the 'overload titration' method. We obtained a linear relationship between observed and calculated $[Fe^{3+}]$ ($\log[Fe^{3+}]_{calc}=1.07\pm0.03 \times \log[Fe^{3+}]_{titration} + 8.7\times10^{-20}\pm6.5\times10^{-20}$, $r^2=0.93$, n=98, Figure 2c). The positive intercept implies a slight systematic overestimate of $FeNN_3$ by the ion pairing model, which is supported by the relationship between the proportion of Fe bound to $FeNN_3$ and the HNN concentration (Figure 2d). The observed proportion of Fe(III) that was detected as $FeNN_3$ at both 1 and 5 μmol L^{-1} HNN was thus slightly lower (by an average of 10 and 15 % respectively) than predicted by the ion pairing model. Our calculated side reaction coefficients were $\log\alpha'_{FeNN3,Fe3+}$ = 9.1, 11.2 and 13 for 1, 5 and 20 μmol L^{-1} HNN, respectively. These values compared to a $\log\alpha'_{Fe}$ of 8.95 calculated by the ion pairing model at pH_{NBS} 8.0. The similarity between $\log\alpha'_{FeNN3,Fe3+}$ and $\log\alpha'_{Fe}$ at an HNN concentration of 1 μmol L^{-1} means that hydroxide ions will compete with HNN at our lowest HNN concentration (Figure 2c). Given the low solubility of Fe hydroxides (at pH_{NBS} 8.0 and 293 K, $Fe(OH)_3(s)$ is predicted to form at an $[Fe^{3+}]$ concentration of 7.58×10^{-20} mol L^{-1}, equivalent to pFe(III)′ = 10.2), the relatively high proportion of Fe^{3+} (maximum calculated Fe^{3+} in UV irradiated seawater = 5.7×10^{-18} mol L^{-1}) should theoretically result in formation of $Fe(OH)_3(s)$ at both 1 and 5 μmol L^{-1} HNN concentrations. Nevertheless, the linear relationship between observed and calculated Fe^{3+} suggests that $Fe(OH)_3(s)$ formation did not impact on the determination of $FeNN_3$, possibly because the equilibration time was not long enough to detect a reduction due to $Fe(OH)_3(s)$ (a week was used for determination of ${}^*K_S$ (Liu and Millero, 1999)). If we assume no formation of $Fe(OH)_3(s)$ occurred, then Fe^{3+} concentrations are consistent over the range of pH and HNN values examined here.

We concluded that our experiment - speciation calculation framework was adequately consistent within the time frame of our titration experiments. However, we caution that our experiments are likely not at true equilibrium, and while it was not detectable over the <24-hour equilibration period of our titrations, we cannot completely rule out formation of $Fe(OH)_3(s)$. Although our calculations simplify the complex kinetic and thermodynamic processes that influence chemical Fe speciation in aqueous solutions, we argue that they are sufficiently consistent to be used to investigate the relationship between DOC concentration and Fe speciation predicted by the NICA-Donnan model.

As a final step in the development of our experimental framework for examining the relationship between DOC concentrations and the fit of observed Fe speciation to different sets of NICA parameters, we re-derived the NICA constants from Avendaño et al. (2016). We carried out this re-

derivation to improve upon the empirical nature of the original estimates and to account for the difference in $\log k_{FeNN3,H+}$ used to generate the estimates for the NICA affinity constants reported by Avendaño et al. (2016). When fitting for four parameters ($n_{Fe(III)1}$, $n_{Fe(III)2}$, $\log K_{Fe(III)1}$, $\log K_{Fe(III)2}$) we found that repeated estimations (n>3) using the same initial arbitrary parameter values did not produce reproducible results, likely as a result of overfitting the data set. The value of n_i and its relationship to n_H as described in equation (6) have been related to reaction stoichiometry between H^+ and the metal ion (Hiemstra and van Riemsdijk, 2006), thus determination of n_i requires experimental data with sufficient density and range in pH space (Zhu et al., 2021). Unfortunately, we found that this criterion was not satisfied by the data of Avendaño et al. (2016), since titrations at only 3 pH values within a relatively restricted range (less than one pH unit) were undertaken. We therefore initially set the value for $n_{Fe(III)1}$ to 0.31 based on previously reported values available for marine organic matter (Avendaño et al., 2016; Gledhill et al., 2015; Hiemstra and van Riemsdijk, 2006). The value of $n_{Fe(III)2}$ was calculated using the formula $n_2 = 0.76 \times n_1$ which has previously been shown to describe the covariance between n_1 and n_2 observed for multiple cations (Milne et al., 2003). Our re-derived NICA affinity constants (set C) are presented in Table 1 along with a further two sets of constants (sets A and B) taken from the literature (Gledhill et al., 2015; Hiemstra and van Riemsdijk, 2006). As expected, the combination of fixing n_i, the mathematical rederivation and the change in $\log k_{FeNN3,H+}$, resulted in differences in the derived $\log K_{Fe(III)1}$ and $\log K_{Fe(III)2}$ used in this study compared to the values empirically estimated (0.26, 3.6, 0.23 and 8.3 for $n_{Fe(III)1}$, $\log K_{Fe(III)1}$, $n_{Fe(III)2}$, $\log K_{Fe(III)2}$ respectively) by Avendaño et al. (2016).We further examined the impact of n_i by increasing the value of n_1 and n_2 (set D) to consider the possibility that marine DOM is less heterogeneous than typically observed for terrestrial organic matter (Lodeiro et al., 2020; Zhu et al., 2021). As well as influencing the effective competition between the metal and protons (Milne et al., 2003), the non-ideality constant influences the relationship between the free metal ion concentration and the total dissolved metal concentration (also termed the concentration dependency, Milne et al. 2003). Incorporation of heterogeneity results in an exponential increase in Fe^{3+} as DFe concentrations increase, which arises because stronger binding sites in the distribution are occupied first. Higher values of n_i result in a shallower exponential curve for the relationship between Fe^{3+} and DFe concentrations.

Table 1. Four sets of constants for Fe(III) binding to the two dissolved organic matter binding site types of the NICA-Donnan model. Parameter sets A and B were taken from the literature, Hiemstra and van Riemsdijk (2006) and Gledhill et al. (2015), respectively. Parameter sets C and D were re-derived for this study based on raw titration data obtained in Celtic Sea samples previously reported in Avendaño et al. (2016). We fixed the non-ideal constants ($n_{Fe(III)}$) to derive the binding affinity ($\log K_{Fe(III)}$) for both parameter sets C and D. The goodness of fit is indicated as root mean square error (RMSE).

Fe(III) NICA constants	set A	set B	set C	set D
Carboxylic-type groups				
$\log K_{Fe(III)1}$	2.8	3.6	2.81±0.36	3.16±0.001
$n_{Fe(III)1}$	0.36	0.3	0.31	0.4
Phenolic-type groups				
$\log K_{Fe(III)2}$	8.3	11.2	9.04±0.01	9.80±0.01
$n_{Fe(III)2}$	0.23	0.15	0.24	0.3
RMSE for parameters rederived in this study	NA		0.7908	0.2149

Influence of dissolved organic carbon concentration on determined and calculated Fe speciation at constant pH

In this work, we analyzed 106 samples from three cruises undertaken in November (DY018, 47 samples), April (DY029, 34 samples) and July (DY033, 28 samples) by CLE-AdCSV and present raw titration data in the SI (Supplementary Figure S2). We first compared $FeNN_3$ concentrations calculated with the NICA-Donnan model using parameter sets A-D with the observed $FeNN_3$ concentrations for the whole data set (Table 2, Supplementary Figure S3). Simulated $FeNN_3$ using parameter set B systematically underestimated the observed $FeNN_3$ concentrations, resulting in a larger RMSE in comparison to sets A, C and D (Table 2). Parameter set B thus overestimated the binding strength of organic matter in our study region. The stronger binding represented by

parameter set B could reflect the estuarine nature of the samples used for the parameter estimation, which might be more strongly influenced by terrestrial organic matter. However, we caution that the data set used for the estimation in Gledhill et al. (2015) was based on analysis of one sample and the authors of that study emphasized that it was intended as a proof of concept.

Table 2. Relationships between calculated (y) and observed (x) $FeNN_3$ concentrations obtained using four sets of NICA constants. Sets A and B and are taken from the literature, Hiemstra and van Riemsdijk (2006) and Gledhill et al. (2015), respectively. Sets C and D were re-derived for this study based on titrations data taken from Avendaño et al. (2016). The number of observations (n) was 643. The goodness of fit is indicated as root mean square error (RMSE).

Fe(III) NICA constants	set A	set B	set C	set D
Linear equation	y=1.03x+0.36	**y**=8.05x-0.79	y=1.03x+0.50	y=1.03x+0.39
r^2	0.85	0.78	0.84	0.85
RMSE (nmol L^{-1})	0.95	1.52	0.89	0.98

$FeNN_3$ is a dominant species at 5 and 20 µmol L^{-1} HNN in our titration experiments, and variability in less abundant species might be expected to be more sensitive to changes in binding site concentrations and better highlight systematic bias with respect to DOC concentrations. Therefore, we next compared the relationship between $[Fe^{3+}]_{titration}$ and total Fe with calculated values for Fe^{3+} obtained from combining the ion-pairing and NICA model ($[Fe^{3+}]_{NICA}$) using our four sets of NICA constants for samples binned into three different DOC concentrations: 45-55, 55-65, and >65 µmol L^{-1} (Figure 3). The DOC bins broadly align with concentrations typically observed for semi-refractory, semi-labile and labile DOC respectively (Hansell, 2013), although the division between the different DOC fractions is likely less well defined than implied here. Figure 3 shows that the relationship between $[Fe^{3+}]_{titration}$ and total Fe was quite well described by A, C and D, but not well described by parameter set B, although some differences between Fe^{3+} at 1 µmol L^{-1} HNN at low total Fe concentrations was evident for all sets at DOC concentrations > 55 µmol L^{-1}. Accurate determination of Fe^{3+} concentrations at low total Fe concentrations appears to be an issue for other voltammetric methods used for analysis of Fe speciation (Gerringa et al., 2021) and could be especially

problematic when using HNN as an added ligand because of its lower sensitivity (Ardiningsih et al., 2021). Results of correlation between $[Fe^{3+}]_{titration}$ and $[Fe^{3+}]_{NICA}$ are given in Table 3. Calculated $[Fe^{3+}]_{NICA}$ using parameter sets A, C and D again showed better agreement with $[Fe^{3+}]_{titration}$ (Table 3) than parameter set B. Combining information from intercept, slope and r^2 and Akaike Information Criteria (AIC), A and D were found to be a better fit to the data than C.

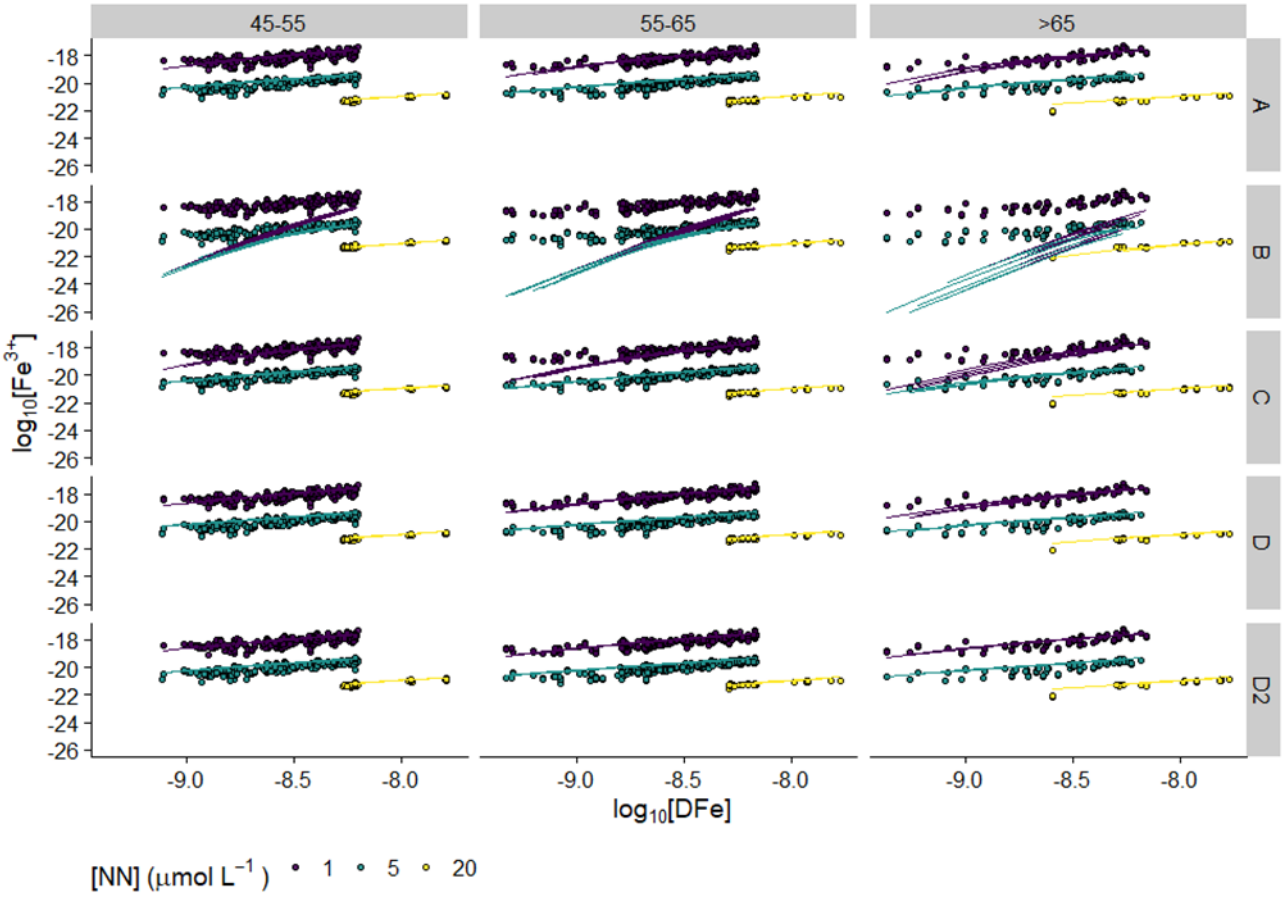

Figure 3. Plots of Fe^{3+} versus total Fe concentrations obtained for titrations binned into three DOC concentration ranges (45-55, 55-65 and >65 µmol L^{-1}). Points show Fe^{3+} concentrations obtained from measured $FeNN_3$ concentrations at three different HNN concentrations: 1, 5 and 20 µmol L^{-1}. Lines show Fe^{3+} concentrations calculated using the NICA-Donnan model combined with an ion-pairing model. Four different NICA parameter sets were applied: parameter set A was reported in Hiemstra and van Riemsdijk, (2006), B in Gledhill et al. (2015), whilst C and D were re-derived for this study based on titration data from Avendaño et al. (2016) (Table 1). Scenario D2 used NICA parameter set D, but assumed that DOC concentrations were constant at 43.7 µmol L^{-1}. Total number of observations = 1489.

We noted that goodness-of-fit of $[Fe^{3+}]_{NICA}$ to $[Fe^{3+}]_{titration}$ tended to decrease with increasing DOC concentration (Table 3). We therefore further examined the scenario that binding sites did not scale with DOC concentration by calculating the Fe speciation using parameter set D and fixing the DOC concentration to the lowest value observed in our study (43.7 µmol L^{-1}). We found similar goodness-of-fit results for this fixed-DOC scenario (D2) across the whole range of DOC concentrations

observed in our study, suggesting that binding sites are not necessarily more abundant at higher DOC concentrations.

Table 3. Correlations of $\log[Fe^{3+}]_{titration}$ (x) observed in titrations undertaken at different HNN concentrations with $\log[Fe^{3+}]_{NICA}$ (y) calculated using a combined ion-pair/NICA-Donnan model. Sets A and B and are taken from the literature, Hiemstra and van Riemsdijk (2006) and Gledhill et al. (2015), respectively. Sets C and D were rederived for this study based on titration data taken from Avendaño et al. (2016). The D2 scenario used parameter set D but assumed a constant DOC concentration of 43.7 µmol L^{-1}.

DOC concentration (µmol L^{-1})	NICA parameter set	Intercept	Slope	R^2	AIC
45-55 (n=612)	A	-1.21±0.16	0.93±0.01	0.95	-55
	B	-10.8±0.6	0.50±0.03	0.27	1655
	C	-2.67±0.18	0.85±0.01	0.93	116
	D	-1.24±0.16	0.93±0.01	0.96	-80
	D2	-1.05±0.16	0.93±0.01	0.96	-89
55-65 (n=643)	A	-1.34±0.14	0.92±0.01	0.96	-138
	B	-10.0±0.8	0.55±0.03	0.23	2008
	C	-2.83±0.2	0.85±0.01	0.91	289
	D	-1.38±0.14	0.92±0.01	0.97	-202
	D2	-1.04±0.13	0.93±0.01	0.97	-249
65-200 (n=234)	A	-2.06±0.32	0.89±0.02	0.92	117
	B	-13.1±1.7	0.43±0.09	0.09	881
	C	-4.20±0.48	0.79±0.03	0.80	303
	D	-2.04±0.29	0.89±0.01	0.94	62
	D2	-1.18±0.25	0.92±0.01	0.96	-16

For our final assessment employing our titration data, we examined the relationship between the non-labile Fe concentrations (DFe*) and $[Fe^{3+}]_{titration}$ observed in our titrations and compared the

relationship to values calculated using the NICA model. For both titration data and simulated results using the NICA-Donnan model, DFe* was calculated using equation (4); as the HNN concentration decreases, the portion of the Fe bound to hydroxides becomes an increasingly more important component of DFe*. Figure 4 shows the relationship between DFe* and Fe^{3+} of measured ($DFe^*_{titration}$) and calculated data (DFe^*_{NICA}), binned according to DOC concentration. The overload titration method assumes that DFe* will be negligible at 20 µmol L^{-1} HNN, and indeed we rarely observed DFe* values greater than 11 % of total Fe (the threshold of uncertainty) at this HNN concentration and so DFe* values are only shown for 1 and 5 µmol L^{-1} NN values. We observed larger scatter in the calculations of DFe* at each HNN concentration compared to that observed for $\log_{10}(Fe^{3+})$ (Fig. 3) and weak correlations ($r^2 < 0.2$, data not shown) between $DFe^*_{titration}$ and DFe^*_{NICA}, which likely reflects increased error propagation for the calculation of DFe*. However, for the most part, observed $DFe^*_{titration}$ overlapped with parameter sets A, C and D and predicted values were thus in the range of observed values. We note that at 5 µmol L^{-1} HNN, concentrations of $[FeNN_3]_{calc}$ were overestimated in our UV seawater experiments (Figure 2d), which could contribute further to discrepancies between $DFe^*_{titration}$ and DFe^*_{NICA}. The analytical limitations of CLE-AdCSV should also be considered here, since its results are known to be influenced by the estimation of sensitivity, lack of equilibrium conditions, and the number and distribution of titration points (Gledhill and Gerringa, 2017; Hudson et al., 2003; Pižeta et al., 2015; Town and Filella, 2000). In particular, the calculation of DFe* is sensitive to bias in estimation of the slope (Hudson et al., 2003), and the ability to detect significant concentrations of DFe* is strongly influenced by the sensitivity of the method. In our case, we note that HNN is one of the least sensitive ligands that can be used to detect Fe by CLE-AdCSV (Ardiningsih et al., 2021), although it has the advantage that it forms one dominant species (Waska et al., 2016), which simplifies application over a range of added ligand concentrations (Abualhaija and van den Berg, 2014). Importantly, the $FeNN_3$ complex can also be detected over a relatively wide pH range (van den Berg, 1991), allowing speciation analysis to be applied over a range of pH values (Avendaño et al., 2016; Gledhill et al., 2015).

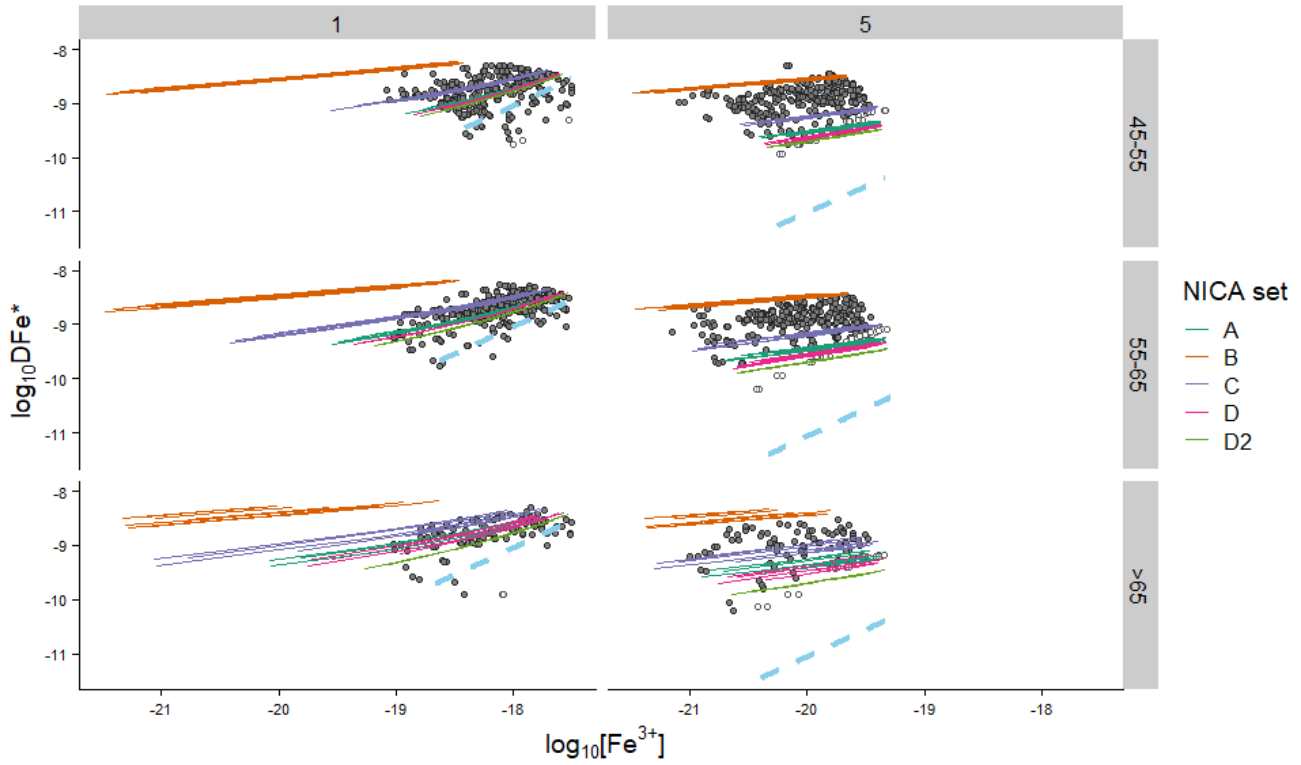

Figure 4. Plot of DFe (i.e. total Fe - $FeNN_3$) versus Fe^{3+} concentrations. Calculated DFe* and Fe^{3+} from titrations are shown as grey points. Only data from 1 and 5 µmol L^{-1} HNN are shown since, in the overlaod titration method, DFe* is assumed to be negligible at 20 µmol L HNN. Open symbols show values where DFe* was below detection and are set to the value of the detection limit. Solid Lines show values predicted for each titration using the NICA-Donnan parameter sets (A-D), at pH 8.0 and temperature 20° C with ambient DOC concentrations. Scenario D2 is the same as set D but a DOC concentration of 43.7 µmol L^{-1} was applied to all samples. The dashed line shows the calculated DFe* in the absence of DOM for reference. The horizontal facet corresponds to the HNN concentration (µmol L^{-1}) and vertical facet bins DFe* and Fe^{3+} concentrations observed and calculated under the different scenarios according to their ambient DOC concentration (µmol L^{-1}).*

Taken together, the calculated $[Fe^{3+}]_{NICA}$ values in our titrations suggest parameter sets A and D provide the best approximations of $[Fe^{3+}]_{titration}$. Examination of DFe* suggests that NICA parameters A, C and D predict DFe* within the range of observed values. Considering NICA sets A and D, binning the data into three different DOC concentrations showed that goodness of fit decreased slightly with increasing DOC concentration (Table 3). The increase in negative intercept with increased DOC concentration suggests that this was because the NICA model slightly overestimated Fe binding to DOM at higher DOC concentrations, and this effect was largely eliminated by assuming a constant DOC concentration of 43.7 µmol L^{-1} with scenario D2. The overestimation of the impact of increasing DOC concentrations could point to dilution of the Fe-binding functional groups by input of autochthonous marine DOM with a lower binding site density. Since the main source of autochthonous marine DOM in our study area is phytoplankton (Carr et al., 2018; Davis et

al., 2018), this would imply that the overall binding affinity of DOM produced by phytoplankton is lower than the aged DOM pool. There is a paucity of data investigating the acid-base binding characteristics of marine DOM, so we recommend further investigation of total binding site concentrations and binding site heterogeneity as a function of DOM mass (Lodeiro et al., 2020), particularly with respect to the changes in DOM composition as a function of productivity. Furthermore, we recommend that alternative experimental designs for titrations are explored for their ability to derive intrinsic, rather than conditional, metal binding constants (e.g. titrations over a wider range of pH values (Avendaño et al., 2016; Gledhill et al., 2015) or with higher pH resolution (Zhu et al., 2021)).

Prediction of Fe(III) speciation in the Celtic Sea using ambient pH and dissolved organic carbon concentrations

The combined impact of variability in pH and DOC concentration and choice of NICA constants on calculated Fe speciation.

For a heterogeneous group of binding sites, DFe, pH, and DOC all influence pFe(III)´. We illustrate the relative importance of the key parameters for driving variability in pFe(III)´ with model experiments (Figure 5a and b). We calculated pFe(III)´ with three scenarios based on the minimum and maximum observed values for pH and DOC we encountered in our study area: i) pH_{NBS} = 8.1, DOC = 45 µmol L^{-1} ii) pH_{NBS} = 8.3, DOC = 45 µmol L^{-1} and iii) pH_{NBS} = 8.3, DOC = 150 µmol L^{-1}. We compare these scenarios with values calculated using ambient pH and DOC, without considering the formation of $Fe(OH)_3(s)$. The different scenarios show that the DOC range encountered in our study area has a greater potential impact on pFe(III)´ than pH does, especially for parameter set D, where scenarios (i) and (ii) overlap. The low impact of pH arises because pH did not vary greatly in the study region (range of ~0.2) and because the lower heterogeneity described by parameter set D reduced the impact of pH.

We compared the data points and the solid curve in Figure 5 (a) and (b) and observed a decrease in pFe(III)´ of approximately 1 and 0.5 log units at our lowest DFe concentrations and 2 and 1 log units at our highest DOC concentrations for parameter sets A and D, respectively. These values provide an estimate of the likely error in pFe(III)´ introduced by scaling to DOC and, not surprisingly, show that the greatest impact will occur at the highest DOC concentrations (Table 1). The differences between the magnitude of the estimates for sets A and D relate to the degree of heterogeneity, as described by

the non-ideality constant, with set D describing a less heterogeneous distribution of binding sites than set A.

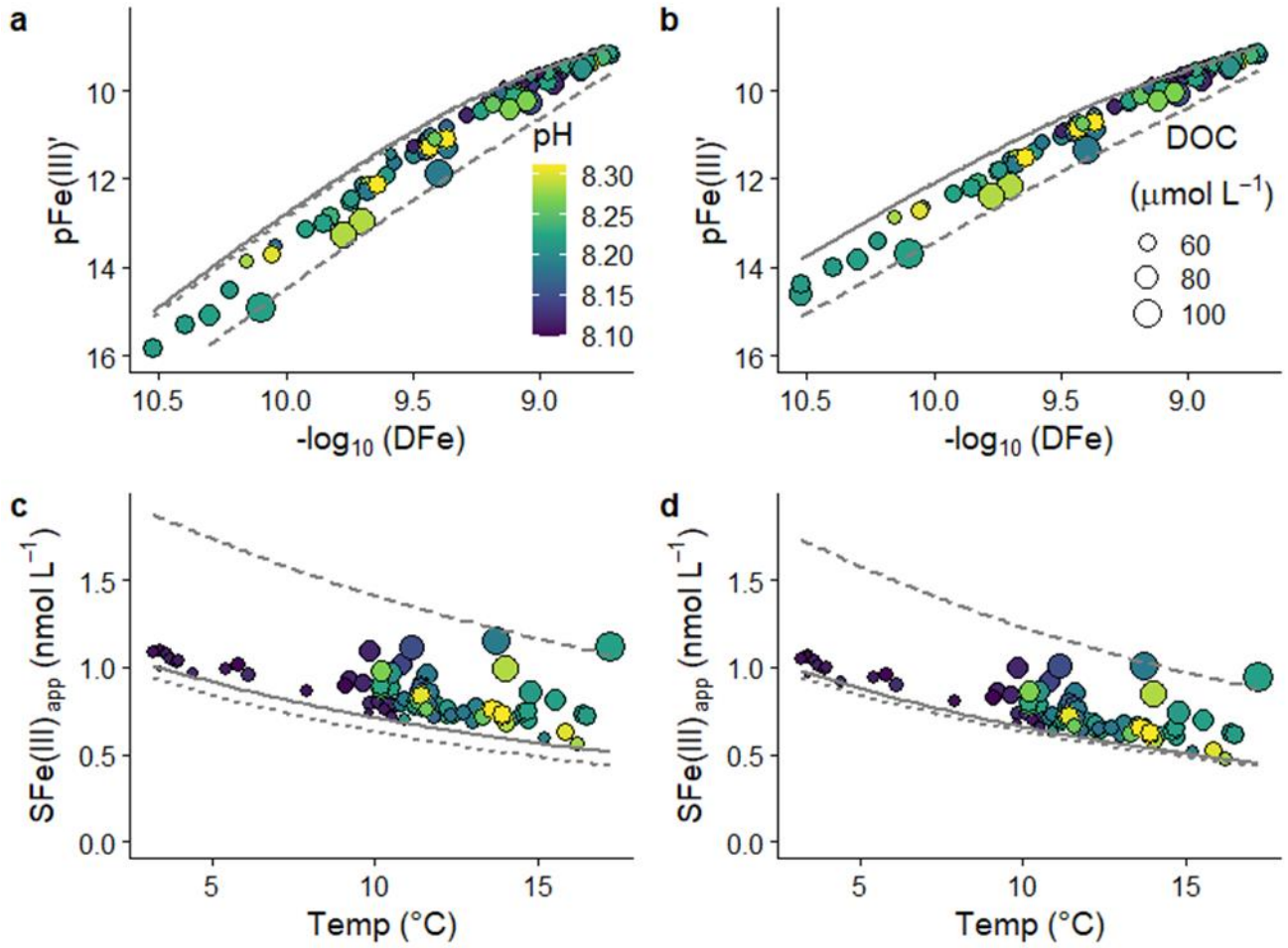

Figure 5 (a), (b) Plots of pFe(III)' as a function of dissolved Fe concentration (DFe) and (c),(d) apparent Fe(III) solubility ($SFe(III)_{app}$) as a function of temperature for NICA parameter sets A and D respectively. The impact of pH and DOC concentration are shown by the colour and size of the points, respectively. The lines show the trend if pH and DOC are assumed constant at (i) solid line: pH = 8.09 and DOC =43.7 µmol L^{-1} (ii) short dashes: pH = 8.31 and DOC =43.7 µmol L^{-1} and (iii) long dashes: pH = 8.31 and DOC =150 µmol L^{-1}.

Impact of pH, DOC and temperature on apparent Fe(III) solubility in the Celtic Sea

Fe(III) solubility strongly influences the overall Fe inventory in the ocean (Johnson et al., 1997) and in the absence of ligands the oceanic DFe inventory would be significantly lower (Hunter and Boyd, 2007; Liu and Millero, 2002). Previous work has suggested that the ocean is saturated with respect to Fe(III) hydroxide (Byrne & Kester, 1976; Kuma et al., 1996, 1998, 2003). However, CLE-AdCSV determinations suggested that ligand concentrations are in excess of DFe, which implies that Fe(III) hydroxide might be undersaturated at the pH of the measurement (Caprara et al., 2016). The saturation state of Fe in the ocean is thus subject to some uncertainty. Furthermore, the interplay

between scavenging and solubility is poorly constrained (Tagliabue et al., 2016), and the potential impact of changes in ambient seawater pH on Fe solubility has rarely been considered (Millero et al., 2009; Ye et al., 2020).

Our calculations of [Fe^{3+}] at the ambient pH and DOC concentrations described above resulted in a maximum value of 4.5×10^{-19} nmol L^{-1} for both parameter sets A and D, obtained at the highest DFe concentration of 1.9 nmol L^{-1}. At pH_{NBS} 8.0 and 20°C, our ion pairing model predicts formation of $Fe(OH)_3(s)$ at an Fe^{3+} concentration of 7.58×10^{-20} mol L^{-1}. Therefore our predicted Fe^{3+} concentrations were oversaturated with respect to $Fe(OH)_3(s)$. We therefore used iterative speciation calculations to investigate the potential interaction between Fe(III) solubility, temperature, pH and Fe binding to DOM in our study area. We calculated apparent Fe(III) solubility ($SFe(III)_{app}$) by setting the total Fe(III) concentrations to 10 nmol L^{-1} for all samples in the model, thereby ensuring formation of the insoluble $Fe(OH)_3(s)$ species. $SFe(III)_{app}$ was then expressed as the sum of the concentrations of aqueous inorganic Fe(III) species and Fe(III) bound to DOM.

Figure 5 (c) and (d) shows the variation of calculated $SFe(III)_{app}$ plotted as a function of temperature for parameter sets A and D respectively. Trends for $SFe(III)_{app}$ for both parameter sets were similar and the highest $SFe(III)_{app}$ was observed at maximum DOC concentrations. Whilst DOC was an important influence on $SFe(III)_{app}$, decreased temperature and pH also both lead to increasing $SFe(III)_{app}$ as a result of changes in the hydrolysis according to equation (1) (Figure 5, c and d). We assessed the relative importance of pH and temperature by calculating $SFe(III)_{app}$ using the same scenarios described for calculation of pFe(III)´ (section 4.3.2). We observed that pH had a greater impact on $SFe(III)_{app}$ than on pFe(III)´. However, in the scenario where Fe binding does scale with DOC concentration, DOC was more important than pH for our study area.

Comparisons between NICA parameter sets A and D showed that $SFe(III)_{app}$ was 0.05 nmol L^{-1} higher for parameter set A than for parameter set D at our lowest DOC concentration (43.7 µmol L^{-1}) and 0.2 nmol L^{-1} higher at our highest DOC concentration (111 µmol L^{-1}) (Figure 5, c and d). The difference was driven by changes in the affinity constant and the relative non-ideality of the binding sites, which effectively results in a lower binding affinity for parameter set D in comparison to parameter set A.

762 Both parameter sets predict maximum $SFe(III)_{app}$ values (1.2 and 1.1 nmol L^{-1}) that are lower than
763 the determined maximum DFe concentrations (1.9 nmol L^{-1}). We emphasize that absolute values
764 have to be compared with caution because of systematic errors in the calculations from e.g. ionic
765 strength corrections. Here, we also need to consider the influence of physical size and filter size cut-
766 off, since the solubility product used in this study was determined using 0.02 µm filter cut off (Liu
767 and Millero, 1999), whilst Fe binding characteristics were determined with a 0.2 µm filter cut off
768 range and DOC concentrations used in this study were determined in the <0.7 µm fraction. We note
769 that fresh Fe hydroxide nanoparticles can be as small as 2-3 nm (Cismasu et al., 2011; Janney et al.,
770 2000) and would thus be classed as dissolved when a 0.02 µm filter cut off is employed, although Fe
771 rich inorganic colloids are potentially negligible in seawater due to rapid flocculation at seawater
772 ionic strength (Gunnars et al., 2002; Krachler et al., 2012). In addition, scavenging processes in
773 which DFe is potentially reversibly adsorbed onto solid phases present in the water column are
774 thought to be an important influence on DFe concentrations (Achterberg et al., 2018; Fitzsimmons et
775 al., 2017) but are not considered in our approach. It is therefore difficult to precisely map our
776 predicted $SFe(III)_{app}$ onto DFe concentrations. Nevertheless, we considered being able to predict
777 $SFe(III)_{app}$ to within 58 % of the determined DFe concentration as encouraging and hence further
778 examined the temporal and spatial variability of Fe species calculated at ambient pH, DFe and DOC
779 in the Celtic Sea.
780
781 <u>Calculated Fe speciation at ambient pH and temperature in the Celtic Sea</u>
782 We examined spatial and temporal variability in Fe speciation that results from changes in DFe and
783 pH in our study region using parameter set D. However, we note that the differences in both
784 calculated pFe(III)´ and $SFe(III)_{app}$ between A and D were limited (maximum for pFe(III)´ of 1.2 log
785 units and 0.2 nmol L^{-1} for $SFe(III)_{app}$), especially at low DOC concentrations (negligible for pFe(III)´
786 and 0.05 nmol L^{-1} for $SFe(III)_{app}$). We re-calculated Fe speciation using ambient DFe concentrations
787 and allowed for formation of $Fe(OH)_3(s)$ where DFe > $SFe(III)_{app}$. We first examined the temporal
788 variability in $SFe(III)_{app}$ and pFe(III)´ on the Celtic Sea Shelf and then spatiotemporal variation
789 across the shelf break using i) ambient DOC and ii) a fixed DOC concentration set to the lowest
790 deep-water DOC concentration observed in our study area (43.7 µmol L^{-1}).
791
792 <u>Seasonal variability in the Central Celtic Sea (site CCS) on the shelf.</u>

The hydrography and the seasonal cycles of DFe, DOC and pH of the Celtic Sea during our sampling period has been described in detail elsewhere (Birchill et al., 2017; Carr et al., 2018; Humphreys et al., 2019; Rusiecka et al., 2018). Briefly, DFe concentrations varied both in the surface mixed layer and deeper waters, with the spring bloom resulting in significant drawdown of DFe in surface waters (0.08 ± 0.01 nmol L^{-1}, n= 2) to levels similar to observations in open ocean regions, while in deeper waters DFe increased from 0.82 ± 0.02, n= 3 (April) to 1.48 ± 0.06 nmol L^{-1}, n= 3 (July) (Birchill et al., 2017). In the surface mixed layer, DOC concentrations were highest in April (73.3 ± 2.9 µmol L^{-1}, n= 3) and lowest in July (57.7 ± 4.0 µmol L^{-1}, n= 5) (Figure S4). DOC concentrations tended to decrease with increasing depth in April and November, and concentrations in all three samples below the thermocline were 64.8 ± 0.0 µmol L^{-1} (n= 3) in April and 58.7 ± 1.8 µmol L^{-1} (n= 4) in November. In July, the trend of DOC was opposite, such that above the thermocline DOC decreased with increasing depth, whilst higher DOC was observed below the thermocline (67.6 ± 4.6 µmol L^{-1}, n= 2). pH was higher in surface waters compared to deeper waters during all three sampling campaigns (Figure S4). A vertical gradient in pH was observed in November with a difference of 0.11 between the surface mixed layer and below the mixed layer.

The changes in DFe, pH and temperature throughout the seasonal cycle resulted in changes in both $SFe(III)_{app}$ and pFe(III)´ (Figure 6). In surface waters in July and November, DFe was consistently lower than calculated $SFe(III)_{app}$ and as expected, DFe was thus undersaturated with respect to $Fe(OH)_3(s)$ formation in our calculations (Figure 6a). Below the mixed layer (>75 m), remineralization of sinking organic matter in the bottom mixed layer resulted in increased DFe (Birchill et al., 2017) and formation of $Fe(OH)_3(s)$ in our calculations (Figure 6a). With the constant DOC scenario, $SFe(III)_{app}$ changed by < 0.03 nmol L^{-1} at station CCS. For the ambient DOC scenario $SFe(III)_{app}$ was overall higher by 0.3 nmol L^{-1} as a result of the increased DOC concentrations (Figure S4), however variability was also low (<0.02 nmol L^{-1}). We found that the $SFe(III)_{app}$ determined by our speciation model for the bottom mixed layer were very similar (0.54-0.87 nmol L^{-1}, Figure 6a) to the concentrations of DFe determined throughout the well-mixed water column in April (0.82 ± 0.04 nmol L^{-1}, n=6). Our results therefore suggest that when the water column is stratified, water below the mixed layer is oversaturated with Fe as a result of constant supply of DFe by remineralization. Winter mixing subsequently resets the DFe inventory to one that our results suggest could be based on Fe solubility.

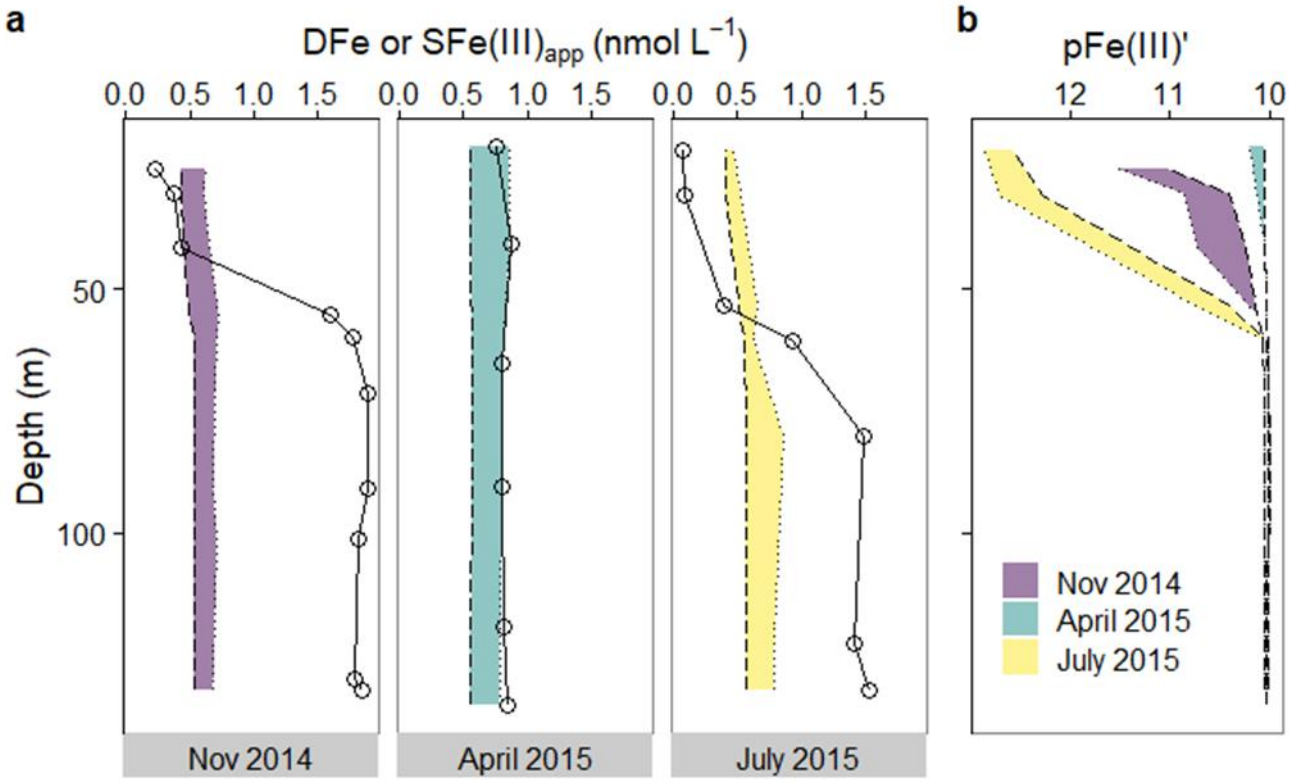

Figure 6. (a) Seasonal changes in the vertical distribution of observed dissolved Fe (<0.2 µm, point and solid line) and calculated apparent Fe(III) solubility ($SFe(III)_{app}$ = Fe(III)'+Fe bound to DOM) using NICA parameter set D. Lines show values calculated using a fixed DOC concentration of 43.7 µmol L^{-1} (long dashes) or ambient DOC concentration (dotted line) and the shaded area highlights the difference between the two scenarios. For calculation of $SFe(III)_{app}$, we assumed a total Fe(III) concentration of 10 nmol L^{-1} in our calculations and DFe was therefore not an input parameter in the calculations. (b) pFe´ ($-\log_{10}$(Fe(III))) was calculated allowing for the formation of ferrihydrite when DFe was greater than $SFe(III)_{app}$ with ambient (dots) and fixed (dashes) DOC concentration scenarios. Calculations were performed using ambient pH and temperature for samples collected on the shelf in autumn (November 2014), spring (April 2015) and summer (July 2015).

Above the mixed layer, pFe(III)´ was primarily dependent on DFe concentrations, with pH having a minor influence (Figure 6b) because of the low degree of heterogeneity predicted by parameter set D (Figure 5b). Below the surface (>75 m), the over-saturation of Fe in July and November meant that pFe(III)´ was rather constant (10.04±0.02) and controlled by the formation of $Fe(OH)_3$(s) in our calculations rather than by the strength of binding to organic matter. In April, surface water (<75 m) pFe(III)´ was similar to those in deeper waters as the water column was well-mixed, whilst a marked increase of pFe(III)´ was observed from surface to deeper waters in July and November (Figure 6b). pFe(III)´ was thus predicted to increase in surface waters from summer through to spring in both constant and ambient DOC scenarios. The increase in pFe(III)´ was thus largely driven by the drawdown of DFe in April resulting from phytoplankton productivity (Birchill et al., 2017). After July, the slight increase in vertical exchange due to mixing and the on shelf circulation pattern

resulted in a decrease surface water pFe(III)´ from July to November, even though the water column remained stratified.

Spatiotemporal variation in key variables and Fe speciation over the Shelf break

Temperature and salinity data over the shelf break are provided in Figure S5. Dissolved Fe ranged in concentration between 0.03-1.90 nmol L^{-1} along the transect and was lower in surface waters (0.22±0.12 nmol L^{-1} in November, 0.20±0.28 nmol L^{-1} in July), and enhanced in deeper waters below ~500 m (1.04±0.24 nmol L^{-1} in November, 0.87±0.14 nmol L^{-1} in July, Figure 7). The distribution and concentration of DFe are broadly consistent with previous observations in the Celtic Sea (Nedelec et al., 2007) and neighbouring Bay of Biscay (Laès et al., 2007; Ussher et al., 2007). A notable exception is that the DFe observed in this study during July 2015 in the surface mixed layer include the lowest reported DFe concentrations (< 0.1 nmol L^{-1}) for waters in this region. These are attributed to biological Fe uptake during the spring bloom coupled with low external inputs to the surface mixed layer (Birchill et al., 2017). In contrast to surface waters, concentrations of DFe in excess of 1.00 nmol L^{-1} (to a maximum of 1.90 nmol L^{-1}) were observed at inner shelf stations in November (C03-C06, CS2) and July (C04-06) at depths >500 m, which we attribute to a lateral flux of DFe from the Celtic Sea shelf slope (Nedelec et al., 2007).

Average DOC concentrations of 60.1 ± 9.2 µmol L^{-1} (n= 48) were observed in November, and 58.4 ± 14.2 µmol L^{-1} (n= 28) in July (Figure 7). Higher DOC concentrations were occasionally observed in surface waters (station C06 in November (98.23 µmol L^{-1}) and station C02 in July (111 µmol L^{-1})). Between 200-1000 m, DOC was higher at C03 station than at other stations in November, a feature that partly coincided with higher DFe concentrations. In the deep ocean (> 1000 m), DOC was slightly lower in July (49.2±3.19 µmol L^{-1}) than in November (52.3±3.3 µmol L^{-1}).

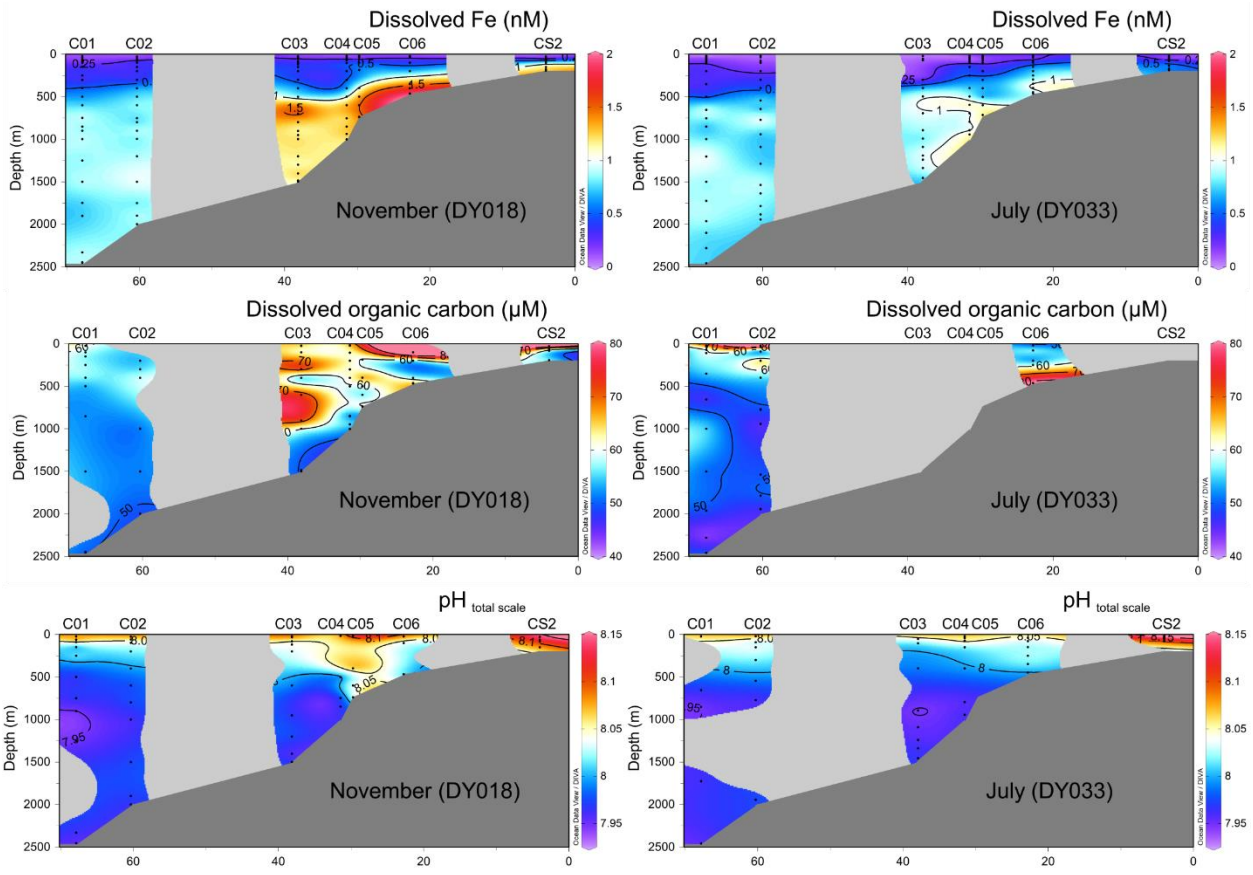

Figure 7. The distribution of dissolved Fe (DFe), dissolved organic carbon (DOC) , pH_{total} (on the total scale) during autumn (DY018, November 2014) and summer (DY033, July 2015) over the shelf break.

Surface waters in the area exhibited higher, relatively uniform pH (Figure 7). Higher surface water pH at C04-06 stations coincided with higher DOC in autumn, which suggest that both of these features were driven by increased productivity as observed at CCS. At depth (> 1000 m), changes in pH corresponded to changes in salinity and temperature and were thus likely influenced by water mass circulation and the biological carbon pump (Figure S5).

For both the ambient and constant DOC scenarios, $SFe(III)_{app}$ was >0.8 nmol L^{-1} in the deep ocean (>1500 m) at stations C01 and C02 in November and July (Figure 8). Mean $SFe(III)_{app}$ (0.96±0.08 and 0.88±0.08 nmol L^{-1} for the ambient and constant DOC scenarios respectively) was again remarkably close to the mean observed DFe concentrations (0.9±0.1 nmol L^{-1}). We emphasize here that the DFe concentration is not a parameter included in the calculations of $SFe(III)_{app}$, since the total Fe concentration is set to 10 nmol L^{-1} for all samples and our calculated $SFe(III)_{app}$ concentrations are thus independent of DFe. The potential impact of scaling to DOC concentration is illustrated by increases in the difference between $SFe(III)_{app}$ calculated where ambient DOC

concentrations were high (>70 µmol L^{-1}) relative to the assumed constant concentration scenario of 43.7 µmol L^{-1} at stations C03-CS2 in November or at station C06 in July (Figure 8). Nevertheless the difference between $SFe(III)_{app}$ calculated at constant DOC and ambient DOC was always less than 0.54 nmol $^{-1}$ (Figure 8) and scaling to DOC thus has a limited overall impact on determined $SFe(III)_{app}$ in shelf waters.

In surface waters, DFe was consistently lower (<0.25 nmol L^{-1}) than $SFe(III)_{app}$ predicted using both DOC scenarios and Fe^{3+} was thus undersaturated with respect to $Fe(OH)_3(s)$ formation in our calculations (Figure 8), as observed for surface waters at CCS. The depth at which DFe became less than $SFe(III)_{app}$ shoaled with the DFe concentration (Figure 7 and 8). In waters close to the seafloor on the inner shelf (C03-C06), DFe concentrations were in excess of the $SFe(III)_{app}$ concentration. As described for station CCS and observed on the Peruvian Shelf (Zhu et al., 2021), we suggest that these waters were influenced by non-equilibrium processes. Our speciation calculations are considered to be at equilibrium and thus do not account for any non-equilibrium processes that may be occurring in the water column, such as remineralization, scavenging, inputs from sediments or changes in redox state. Our study region is known to experience inputs of DFe along with other metals in nepheloid layers that propagate offshore from the sediments over the shelf break (Laès et al., 2007; Rusiecka et al., 2018), and previous work found that the authigenic or scavenged fraction of particulate Fe becomes increasingly important close to the seafloor (Marsay et al., 2017). Such sediment-derived benthic inputs can be expected to be scavenged from the water column and adsorptive processes are likely to depend on particle concentrations (Bergquist and Boyle, 2006; Fitzsimmons et al., 2013; John et al., 2018). However, the mechanisms and processes governing scavenging in the ocean are poorly constrained (Boyd and Ellwood, 2010; Tagliabue et al., 2014) and scavenging rates are effectively treated as “free” parameters in biogeochemical models and thus tuned to achieve realistic Fe concentrations (Tagliabue et al., 2014). Our work confirms previous studies (Hiemstra and van Riemsdijk, 2006) suggesting that the solubility of Fe is an important constraint on the extent of Fe scavenging in the ocean.

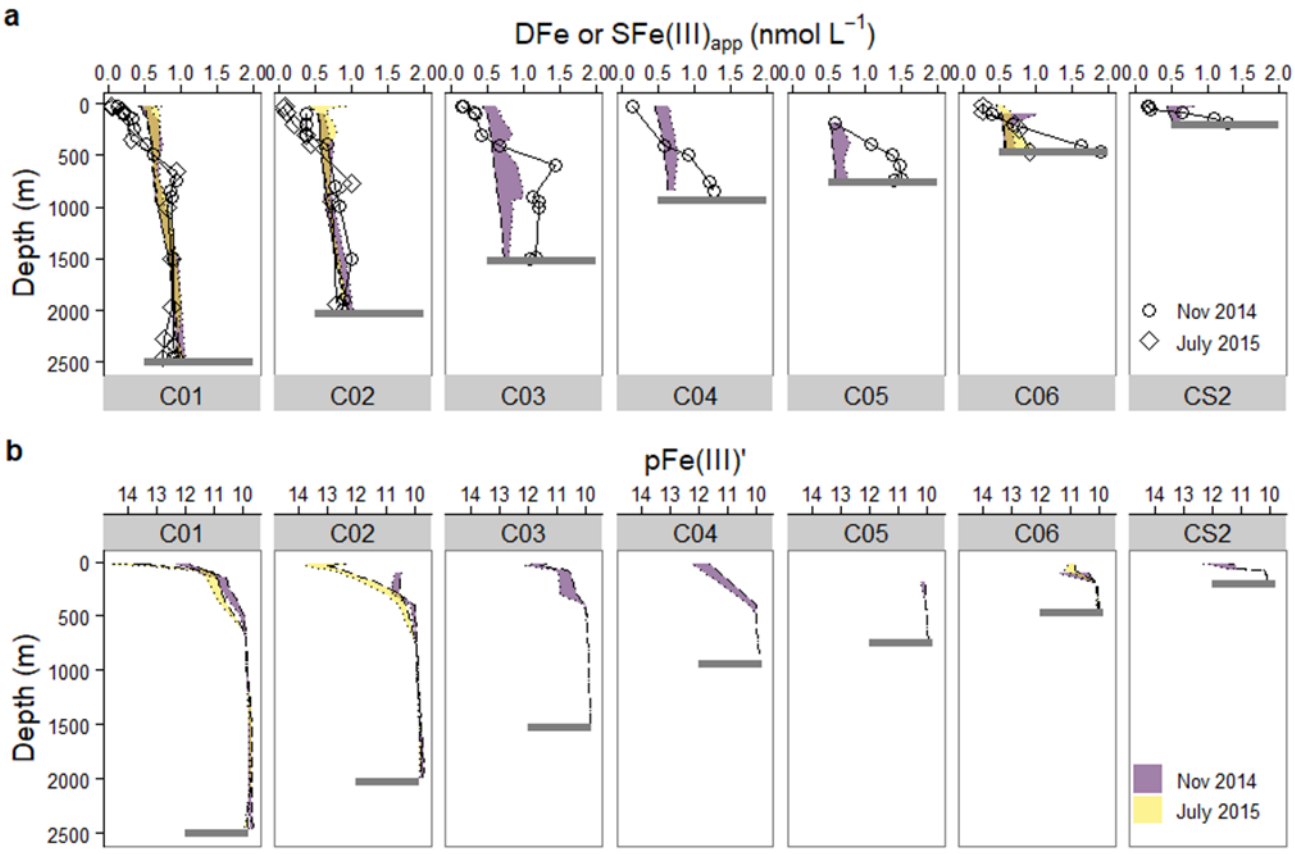

Figure 8. (a) Changes in the vertical distribution of calculated $SFe(III)_{app}$ using NICA parameter set D - observed dissolved Fe (<0.2 µm, point/diamond and solid line) are provided for reference. Lines show values calculated using a fixed DOC concentration of 43.7 µmol L^{-1} (long dashes) or ambient DOC concentration (dotted line) and the shaded area highlights the difference between the two scenarios. For calculation of $SFe(III)_{app}$, we assumed a total Fe(III) concentration of 10 nmol L^{-1} in our calculations and DFe was therefore not an input parameter in the calculations. (b) pFe(III)´ ($-log_{10}$(Fe(III))) was calculated from DFe, or $SFe(III)_{app}$ when DFe > $SFe(III)_{app}$. Calculations applied the ambient pH and temperature for samples collected over the shelf break in autumn (November 2014) and summer (July 2015) seasons. DOC concentrations were not determined for C03-C05 and CS2 in July 2015. Grey bars show the depth of the water column at each station.

Calculated pFe(III)´ was lowest in deep waters and highest in surface waters indicating an increase in Fe(III)´ in deeper waters (Figure 8b, pFe(III)´ scale is reversed). Below ~500m, pFe(III)´ (10.04±0.02) was relatively constant throughout the water column in November and July and irrespective of the DOC scenario, largely because it is set by the solubility product of $Fe(OH)_3$(s) in our calculations (i.e. pFe(III)´ ∝ $[Fe^{3+}]$ which in turn is limited by $Fe(OH)_3$(s)). In surface waters, when pFe(III)´ is dependent on the DFe concentration, pFe(III)´ increased towards the open ocean from a minimum of 10.8 (constant DOC) or 11 (ambient DOC) at C06 to a maximum of 13.2 (constant DOC) or 14.6 (ambient DOC) at C01 (Figure 8). For the stations furthest offshore, the potential impact of scaling to DOC for calculation of pFe(III)´ was more important. For example, a 30 µmol L^{-1} increase in DOC resulted in an increase of two units in pFe(III)´ in surface waters at station C01. We found that values of pFe(III)´ predicted using parameter set D under both constant

and variable DOC scenarios encompassed the range of values found to support both iron-replete and iron-limited growth in families of phytoplankton including cyanophytes, haptophytes and diatoms which have been observed in our study area (Blain et al., 2004). For example, reduction in growth of *Synechococcus* sp. was shown to begin at pFe´ values of 14 (Timmermans et al., 2005), close to the lowest values predicted by parameter set D with ambient DOC concentrations, while Sunda & Huntsman (1995) found onset of growth was limited at 20 pmol L^{-1} (pFe(III)´ = 10.7) for the small haptophyte *Emiliania huxleyi* and at 160 pmol L^{-1} (pFe(III)´ = 9.8) for the diatom *Thallassiosira weissflogii*. However, we have not considered the role of redox chemistry in our calculations. Fe(II) is known to be more readily available to phytoplankton (Shaked and Lis, 2012) and significant concentrations of Fe(II) can be formed via photochemical reduction in surface waters, with Fe(II) concentrations of up to 175 pmol L^{-1} previously reported for surface waters (<50 m) in this region (Ussher et al., 2007).

Conclusions

In this work, we combined analysis of Fe speciation by AdCSV with an ion-pairing/NICA-Donnan model to determine Fe(III) speciation at equilibrium in the Celtic Sea. We first calibrated our competing added ligand (HNN) in the absence of organic matter for the experimental conditions applied in our study. We then compared titration data obtained by varying both Fe concentrations and HNN concentrations with calculations of Fe speciation predicted via the NICA-Donnan model with four sets of parameters and found that the parameter sets that predicted relatively weak binding with low heterogeneity best described our titration data. We further found that fits improved on application of a constant low DOC concentration of 43.7 µmol L^{-1} across the data set, rather than assuming that binding scaled to ambient DOC concentrations. This suggests that binding sites may be more strongly linked to the refractory component of marine DOM and autochthonous marine inputs of DOM that result from phytoplankton productivity may not result in increased binding site concentration or heterogeneity.

We used the NICA-Donnan parameters that fitted most closely to our titration data to predict $SFe(III)_{app}$ and pFe(III)´ at ambient seawater pH and temperature with both ambient and fixed DOC concentrations. Calculated $SFe(III)_{app}$ concentrations (ca. 0.9 nmol L^{-1}) were within the range of the water column DFe concentrations observed on the shelf after winter mixing and also the furthest off-shore deep water DFe concentrations. In surface waters DFe concentrations were lower than

$SFe(III)_{app}$ as result of the drawdown of DFe by phytoplankton. On the shelf in July and November and over the shelf break DFe exceeded $SFe(III)_{app}$ in deeper waters close to the seafloor, which could potentially be ascribed to inputs of DFe from remineralization and/or release from sediments. Although the proximity of our calculated $SFe(III)_{app}$ to the observed DFe concentrations is very encouraging, we highlight that our calculations are a simplification of the real system since we do not account for non-equilibrium processes, and the physical size of our $SFe(III)_{app}$ fraction may not map directly onto the DFe concentration. Comparing the fixed and ambient DOC scenarios suggests that scaling binding site concentrations to DOC concentrations has a limited overall impact on Fe speciation and the impact was mostly restricted to surface waters where DFe concentrations are lower than $SFe(III)_{app}$. Since $SFe(III)_{app}$ is controlled by the solubility of $Fe(OH)_3(s)$, relative changes in $SFe(III)_{app}$ will depend on both pH and temperature. In our study region, changes in temperature resulted in a potential 0.5 nmol L^{-1} change in $SFe(III)_{app}$, whilst the pH range observed in our study area was too limited to detect a strong pH effect. The impact of temperature on Fe speciation therefore deserves further consideration in future studies.

We also calculated pFe(III)´ in our study region and predicted values between 10 and 14, a range which encompasses the range of pFe(III)´ shown to limit growth in phytoplankton. The lower limit on pFe(III)´ was set by the solubility of $Fe(OH)_3(s)$. The upper limit and changes in pFe(III)´ were strongly influenced by the DFe concentration, although DOC concentrations also had an impact if binding site concentrations are scaled to DOC. The limited pH range and low binding site heterogeneity meant that pH did not have a strong influence on pFe(III)´ in this study region.

We suggest that the use of intrinsic binding parameters for Fe binding to DOM has the potential to improve understanding of the influence of organic matter on Fe solubility at ambient pH and temperatures and allow for more confident disentangling of the different processes affecting the DFe inventory, although further work is required to refine NICA constants for Fe in seawater. Furthermore, our results suggest it may be possible to further simplify calculations of Fe speciation in marine waters by assuming a constant binding site concentration, at least in waters remote from terrestrial influences, although this finding should be confirmed in further work employing more sensitive analytical approaches for determination of Fe speciation than we applied in this study. A robust parameterization of the relationship between pH, DOC, temperature and DFe with respect to both Fe bioavailability and solubility also has the potential to provide for a more mechanistic description of Fe binding in global biogeochemical models.

Acknowledgement

The authors would like to thank Bert-Jan Groenenberg for his help with PEST-ORCHESTRA. We thank the captain and crew of the RSS Discovery. KZ was supported by a scholarship from the China Scholarship Council. The project was funded by the UK Natural Environment Research Council (NE/L501840/1 (A.B.), NE/K001779/1 (M.L., S.U., A.M.), NE/K002007/1 (N.C and C.M.), NE/K001973/1 (E.A. and M.G.) and the Helmholtz Association. The authors declare no competing financial interest. All data that supports the findings of this study have been submitted to the British Oceanography Data Centre. Raw titration data can be downloaded from dx.doi.org/10.17504/protocols.io.brc4m2yw.

References

Abualhaija, M.M., van den Berg, C.M.G., 2014. Chemical speciation of iron in seawater using catalytic cathodic stripping voltammetry with ligand competition against salicylaldoxime. Mar. Chem. 164, 60–74. https://doi.org/10.1016/j.marchem.2014.06.005

Achterberg, E.P., Steigenberger, S., Marsay, C.M., Lemoigne, F.A.C., Painter, S.C., Baker, A.R., Connelly, D.P., Moore, C.M., Tagliabue, A., Tanhua, T., 2018. Iron biogeochemistry in the High Latitude North Atlantic Ocean. Sci. Rep. 8, 1–15. https://doi.org/10.1038/s41598-018-19472-1

Apte, S.C., Gardner, M.J., Ravenscroft, J.E., 1988. An evaluation of voltammetric titration procedures for the determination of trace metal complexation in natural waters by use of computer simulation. Anal. Chim. Acta 212, 1–21.

Ardiningsih, I., Zhu, K., Lodeiro, P., Gledhill, M., Reichart, G.-J., Achterberg, E.P., Middag, R., Gerringa, L.J.A., 2021. Iron speciation in the Fram Strait and over the Northeast Greenland Shelf: An inter-comparison study of voltammetric methods. Front. Mar. Sci. 7, 1203. https://doi.org/10.3389/fmars.2020.609379

Avendaño, L., Gledhill, M., Achterberg, E.P., Rérolle, V.M.C., Schlosser, C., 2016. Influence of ocean acidification on the organic complexation of iron and copper in Northwest European shelf seas; a combined observational and model study. Front. Mar. Sci. 3, 58. https://doi.org/10.3389/fmars.2016.00058

Barbeau, K., 2006. Photochemistry of organic iron (III) complexing ligands in oceanic systems. Photochem. Photobiol. 82, 1505–1516. https://doi.org/10.1562/2006-06-16-IR-935

Barrón, C., Duarte, C.M., 2015. Dissolved organic carbon pools and export from the coastal ocean. Global Biogeochem. Cycles 29, 1725–1738. https://doi.org/10.1002/2014GB005056

Benedetti, M.F., van Riemsdijk, W.H., Koopal, L.K., 1996. Humic Substances Considered as a Heterogeneous Donnan Gel Phase. Enviromental Sci. Technol. 30, 1805–1813. https://doi.org/10.1021/ES950012Y

Bergquist, B.A., Boyle, E.A., 2006. Dissolved iron in the tropical and subtropical Atlantic Ocean. Global Biogeochem. Cycles 20. https://doi.org/10.1029/2005GB002505

Birchill, A.J., Milne, A., Woodward, E.M.S., Harris, C., Annett, A., Rusiecka, D., Achterberg, E.P., Gledhill, M., Ussher, S.J., Worsfold, P.J., Geibert, W., Lohan, M.C., 2017. Seasonal iron depletion in temperate shelf seas. Geophys. Res. Lett. 44, 8987–8996. https://doi.org/10.1002/2017GL073881

Blain, S., Guieu, C., Claustre, H., Leblanc, K., Moutin, T., Quéguiner, B., Ras, J., Sarthou, G., 2004. Availability of iron and major nutrients for phytoplankton in the northeast Atlantic Ocean. Limnol. Oceanogr. 49, 2095–2104. https://doi.org/10.4319/lo.2004.49.6.2095

Boyd, P.W., Ellwood, M.J., 2010. The biogeochemical cycle of iron in the ocean. Nat. Geosci. 3, 675–682. https://doi.org/10.1038/ngeo964

Boyd, P.W., Jickells, T., Law, C.S., Blain, S., Boyle, E.A., Buesseler, K.O., Coale, K.H., Cullen, J.J., de Baar, H.J.W., Follows, M., Harvey, M., Lancelot, C., Levasseur, M., Owens, N.P.J., Pollard, R., Rivkin, R.B., Sarmiento, J., Schoemann, V., Smetacek, V., Takeda, S., Tsuda, A., Turner, S., Watson, A.J., 2007. Mesoscale iron enrichment experiments 1993-2005: Synthesis and future directions. Science (80-.). 315, 612–617.

Boye, M., Aldrich, A.P., van den Berg, C.M.G., de Jong, J.T.M., Veldhuis, M., de Baar, H.J.W., 2003. Horizontal gradient of the chemical speciation of iron in surface waters of the northeast Atlantic Ocean. Mar. Chem. 80, 129–143.

Boye, M., van den Berg, C.M.G., de Jong, J.T.M., Leach, H., Croot, P., de Baar, H.J.W., 2001. Organic complexation of iron in the Southern Ocean. Deep. Res. Part I-Oceanographic Res. Pap. 48, 1477–1497.

Buck, K.N., Moffett, J., Barbeau, K.A., Bundy, R.M., Kondo, Y., Wu, J., 2012. The organic complexation of iron and copper: an intercomparison of competitive ligand exchange-adsorptive cathodic stripping voltammetry (CLE-ACSV) techniques. Limnol. Oceanogr. Methods 10, 496–

515. https://doi.org/10.4319/lom.2012.10.496

Buck, K.N., Sedwick, P.N., Sohst, B., Carlson, C.A., 2018. Organic complexation of iron in the eastern tropical South Pacific: Results from US GEOTRACES Eastern Pacific Zonal Transect (GEOTRACES cruise GP16). Mar. Chem. 201, 229–241. https://doi.org/10.1016/J.MARCHEM.2017.11.007

Buck, K.N., Sohst, B., Sedwick, P.N., 2015. The organic complexation of dissolved iron along the U.S. GEOTRACES (GA03) North Atlantic Section. Deep. Res. Part II Top. Stud. Oceanogr. 116, 152–165. https://doi.org/10.1016/j.dsr2.2014.11.016

Byrne, R.H., Kester, D.R., 1976. Solubility of hydrous ferric oxide and iron speciation in seawater. Mar. Chem. 4, 255–274.

Byrne, R.H., Luo, Y.-R.R., Young, R.W., 2000. Iron hydrolysis and solubility revisited: observations and comments on iron hydrolysis characterizations. Mar. Chem. 70, 23–35. https://doi.org/10.1016/S0304-4203(00)00012-8

Caprara, S., Buck, K.N., Gerringa, L., Rijkenberg, M., Monticelli, D., 2016. A compilation of iron speciation data for open oceanic waters. Front. Mar. Sci. 3, 221. https://doi.org/10.3389/FMARS.2016.00221

Carr, N., Davis, C.E., Blackbird, S., Daniels, L.R., Preece, C., Woodward, M., Mahaffey, C., 2018. Seasonal and spatial variability in the optical characteristics of DOM in a temperate shelf sea. Prog. Oceanogr. https://doi.org/10.1016/J.POCEAN.2018.02.025

Cismasu, A.C., Michel, F.M., Tcaciuc, A.P., Tyliszczak, T., Brown Jr, G.E., 2011. Composition and structural aspects of naturally occurring ferrihydrite. Comptes Rendus Geosci. 343, 210–218.

Cutter, G., Casciotti, K., Croot, P., Geibert, W., Heimbürger, L.-E., Lohan, M., Planquette, H., van de Flierdt, T., 2017. Sampling and Sample-handling Protocols for GEOTRACES Cruises. Version 3, August 2017. 139pp. & Appendices. https://doi.org/http://dx.doi.org/10.25607/OBP-2

Davis, C.E., Blackbird, S., Wolff, G., Woodward, M., Mahaffey, C., 2018. Seasonal organic matter dynamics in a temperate shelf sea. Prog. Oceanogr. 177, 101925. https://doi.org/10.1016/J.POCEAN.2018.02.021

Dickson, A.G., 2010. Part 1 : Seawater carbonate chemistry The carbon dioxide system in seawater : equilibrium chemistry and measurements. Guid. to best Pract. Ocean Acidif. Res. data Report. 1–40. https://doi.org/10.2777/66906

Dickson, A.G., 1990. Standard potential of the reaction: AgCl(s) + 12H2(g) = Ag(s) + HCl(aq), and and the standard acidity constant of the ion HSO4− in synthetic sea water from 273.15 to 318.15

K. J. Chem. Thermodyn. 22, 113–127. https://doi.org/http://dx.doi.org/10.1016/0021-9614(90)90074-Z

Dickson, A.G., Millero, F.J., 1987. A comparison of the equilibrium constants for the dissociation of carbonic acid in seawater media. Deep Sea Res. 34, 1733–1743.

Doherty, J., 2019. PEST, Model-Independent Parameter Estimation, User Manual Part I.

Fitzsimmons, J.N., John, S.G., Marsay, C.M., Hoffman, C.L., Nicholas, S.L., Toner, B.M., German, C.R., Sherrell, R.M., 2017. Iron persistence in a distal hydrothermal plume supported by dissolved-particulate exchange. Nat. Geosci. 10, 195–201. https://doi.org/10.1038/ngeo2900

Fitzsimmons, J.N., Zhang, R., Boyle, E.A., 2013. Dissolved iron in the tropical North Atlantic Ocean. Mar. Chem. 154, 87–99. https://doi.org/10.1016/j.marchem.2013.05.009

Gerringa, L.J.A., Gledhill, M., Ardiningsih, I., Muntjewerf, N., Laglera, L.M., 2021. Comparing CLE-AdCSV applications using SA and TAC to determine the Fe binding characteristics of model ligands in seawater [WWW Document]. Biogeosciences Discuss. https://doi.org/10.5194/bg-2021-134

Gerringa, L.J.A., Rijkenberg, M.J.A., Schoemann, V., Laan, P., de Baar, H.J.W., 2015. Organic complexation of iron in the West Atlantic Ocean. Mar. Chem. 177, 434–446. https://doi.org/10.1016/j.marchem.2015.04.007

Gledhill, M., Achterberg, E.P., Li, K., Mohamed, K.N., Rijkenberg, M.J.A., 2015. Influence of ocean acidification on the complexation of iron and copper by organic ligands in estuarine waters. Mar. Chem. 177, 421–433. https://doi.org/http://dx.doi.org/10.1016/j.marchem.2015.03.016

Gledhill, M., Buck, K.N., 2012. The organic complexation of iron in the marine environment: A review. Front. Microbiol. 3, 69. https://doi.org/10.3389/fmicb.2012.00069

Gledhill, M., Gerringa, L.J.A., 2017. The effect of metal concentration on the parameters derived from complexometric titrations of trace elements in seawater—a model study. Front. Mar. Sci. 4, 254. https://doi.org/10.3389/fmars.2017.00254

Gledhill, M., van den Berg, C.M.G., 1994. Determination of complexation of iron(III) with natural organic complexing ligands in seawater using cathodic stripping voltammetry. Mar. Chem. 47, 41–54. https://doi.org/10.1016/0304-4203(94)90012-4

Gunnars, A., Blomqvist, S., Johansson, P., Andersson, C., 2002. Formation of Fe(III) oxyhydroxide colloids in freshwater and brackish seawater, with incorporation of phosphate and calcium. Geochim. Cosmochim. Acta 66, 745–758. https://doi.org/10.1016/S0016-7037(01)00818-3

Gustafsson, J.P., 2001. Modeling the acid–base properties and metal complexation of humic

substances with the Stockholm Humic Model. J. Colloid Interface Sci. 244, 102–112. https://doi.org/http://dx.doi.org/10.1006/jcis.2001.7871

Hansell, D.A., 2013. Recalcitrant dissolved organic carbon fractions. Ann. Rev. Mar. Sci. 5, 421–445. https://doi.org/10.1146/annurev-marine-120710-100757

Hassler, C.S., Alasonati, E., Nichols, C.A.M., Slaveykova, V.I., 2011a. Exopolysaccharides produced by bacteria isolated from the pelagic Southern Ocean - Role in Fe binding, chemical reactivity, and bioavailability. Mar. Chem. 123, 88–98. https://doi.org/10.1016/j.marchem.2010.10.003

Hassler, C.S., Schoemann, V., Nichols, C.M., Butler, E.C. V, Boyd, P.W., 2011b. Saccharides enhance iron bioavailability to Southern Ocean phytoplankton. Proc. Natl. Acad. Sci. U. S. A. 108, 1076–1081. https://doi.org/10.1073/pnas.1010963108

Hiemstra, T., van Riemsdijk, W.H., 2006. Biogeochemical speciation of Fe in ocean water. Mar. Chem. 102, 181–197. https://doi.org/10.1016/j.marchem.2006.03.008

Hogle, S.L., Dupont, C.L., Hopkinson, B.M., King, A.L., Buck, K.N., Roe, K.L., Stuart, R.K., Allen, A.E., Mann, E.L., Johnson, Z.I., Barbeau, K.A., 2018. Pervasive iron limitation at subsurface chlorophyll maxima of the California Current. Proc. Natl. Acad. Sci. U. S. A. 115, 13300–13305. https://doi.org/10.1073/pnas.1813192115

Hudson, R.J.M., Rue, E.L., Bruland, K.W., 2003. Modeling complexometric titrations of natural water samples. Environ. Sci. Technol. 37, 1553–1562. https://doi.org/10.1021/es025751a

Humphreys, M.P., Achterberg, E.P., Hopkins, J.E., Chowdhury, M.Z.H., Griffiths, A.M., Hartman, S.E., Hull, T., Smilenova, A., Wihsgott, J.U., Woodward, E.M.S., Moore, C.M., 2019. Mechanisms for a nutrient-conserving carbon pump in a seasonally stratified, temperate continental shelf sea. Prog. Oceanogr. 177, 101961. https://doi.org/10.1016/j.pocean.2018.05.001

Hunter, K.A., Boyd, P.W., 2007. Iron-binding ligands and their role in the ocean biogeochemistry of iron. Environ. Chem. 4, 221–232. https://doi.org/10.1071/en07012|issn 1448-2517

Hutchins, D.A., Boyd, P.W., 2016. Marine phytoplankton and the changing ocean iron cycle. Nat. Clim. Chang. 6, 1072–1079. https://doi.org/10.1038/nclimate3147

Hutchins, D.A., Bruland, K.W., 1998. Iron-limited diatom growth and Si:N uptake ratios in a coastal upwelling regime. Nature 393, 561–564. https://doi.org/10.1038/31203

Hutchins, D.A., Witter, A.E., Butler, A., Luther III, G.W., 1999. Competition among marine phytoplankton for different chelated iron species. Nature 400, 858–861.

Janney, D.E., Cowley, J.M., Buseck, P.R., 2000. Transmission electron microscopy of synthetic 2-

and 6-line ferrihydrite. Clays Clay Miner. 48, 111–119. https://doi.org/10.1346/CCMN.2000.0480114

Janot, N., Pinheiro, J.P., Botero, W.G., Meeussen, J.C.L., Groenenberg, J.E., 2017. PEST-ORCHESTRA, a tool for optimising advanced ion-binding model parameters: Derivation of NICA-Donnan model parameters for humic substances reactivity. Environ. Chem. 14, 31–38. https://doi.org/10.1071/EN16039

John, S.G., Helgoe, J., Townsend, E., Weber, T., DeVries, T., Tagliabue, A., Moore, K., Lam, P., Marsay, C.M., Till, C., 2018. Biogeochemical cycling of Fe and Fe stable isotopes in the Eastern Tropical South Pacific. Mar. Chem. 201, 66–76. https://doi.org/10.1016/j.marchem.2017.06.003

Johnson, K.S., Gordon, R.M., Coale, K.H., 1997. What controls dissolved iron in the world ocean? Mar. Chem. 57, 137–161.

Kinniburgh, D.G., van Riemsdijk, W.H., Koopal, L.K., Borkovec, M., Benedetti, M.F., Avena, M.J., 1999. Ion binding to natural organic matter: competition, heterogeneity, stoichiometry and thermodynamic consistency. Colloids Surfaces A Physicochem. Eng. Asp. 151, 147–166. https://doi.org/http://dx.doi.org/10.1016/S0927-7757(98)00637-2

Koch, B.P., Ludwichowski, K.U., Kattner, G., Dittmar, T., Witt, M., 2008. Advanced characterization of marine dissolved organic matter by combining reversed-phase liquid chromatography and FT-ICR-MS. Mar. Chem. 111, 233–241. https://doi.org/10.1016/j.marchem.2008.05.008

Kogut, M.B., Voelker, B.M., 2001. Strong copper-binding behavior of terrestrial humic substances in seawater. Environ. Sci. Technol. 35, 1149–1156. https://doi.org/10.1021/es0014584

Krachler, R., Kammer, F. von der, Jirsa, F., Süphandag, A., Krachler, R.F., Plessl, C., Vogt, M., Keppler, B.K., Hofmann, T., 2012. Nanoscale lignin particles as sources of dissolved iron to the ocean. Global Biogeochem. Cycles 26. https://doi.org/10.1029/2012GB004294

Kuma, K., Isoda, Y., Nakabayashi, S., 2003. Control on dissolved iron concentrations in deep waters in the western North Pacific: Iron (III) hydroxide solubility. J. Geophys. Res. C Ocean. 108, 5–1. https://doi.org/10.1029/2002jc001481

Kuma, K., Katsumoto, A., Kawakami, H., Takatori, F., Matsunaga, K., 1998. Spatial variability of Fe(III) hydroxide solubility in the water column of the northern North Pacific Ocean. Deep. Res. 45, 91–113.

Kuma, K., Katsumoto, A., Shiga, N., Sawabe, T., Matsunaga, K., 2000. Variation of size-fractionated

Fe concentrations and Fe(III) hydroxide solubilities during a spring phytoplankton bloom in Funka Bay (Japan). Mar. Chem. 71, 111–123. https://doi.org/10.1016/S0304-4203(00)00044-X

Kuma, K., Nishioka, J., Matsunaga, K., 1996. Controls on iron(III) hydroxide solubility in seawater: The influence of pH and natural organic chelators. Limnol. Oceanogr. 41, 396–407.

Laès, A., Blain, S., Laan, P., Ussher, S.J.J., Achterberg, E.P.E.P., Tréguer, P., De Baar, H.J.W.J.W.W., Laës, A., Blain, S., Laan, P., Ussher, S.J.J., Achterberg, E.P.E.P., Tréguer, P., De Baar, H.J.W.J.W.W., Laes, A., Blain, S., Laan, P., Ussher, S.J.J., Achterberg, E.P.E.P., Treguer, P., De Baar, H.J.W.J.W.W., 2007. Sources and transport of dissolved iron and manganese along the continental margin of the Bay of Biscay. Biogeosciences (BG) 4, 181–194. https://doi.org/10.5194/bg-4-181-2007

Laglera, L.M., Battaglia, G., van den Berg, C.M.G., 2011. Effect of humic substances on the iron speciation in natural waters by CLE/CSV. Mar. Chem. 127, 134–143. https://doi.org/10.1016/j.marchem.2011.09.003

Laglera, L.M., Filella, M., 2015. The relevance of ligand exchange kinetics in the measurement of iron speciation by CLE–AdCSV in seawater. Mar. Chem. 173, 100–113. https://doi.org/10.1016/j.marchem.2014.09.005

Laglera, L.M., Sukekava, C., Slagter, H.A., Downes, J., Aparicio-Gonzalez, A., Gerringa, L.J.A., 2019. First Quantification of the Controlling Role of Humic Substances in the Transport of Iron Across the Surface of the Arctic Ocean. Environ. Sci. Technol. https://doi.org/10.1021/ACS.EST.9B04240

Laglera, L.M., van den Berg, C.M.G., 2009. Evidence for geochemical control of iron by humic substances in seawater. Limnol. Oceanogr. 54, 610–619.

Liu, X., Millero, F.J., 2002. The solubility of iron in seawater. Mar. Chem. 77, 43–54. https://doi.org/10.1016/S0304-4203(01)00074-3

Liu, X., Millero, F.J., 1999. The solubility of iron hydroxide in sodium chloride solutions. Geochim. Cosmochim. Acta 63, 3487–3497. https://doi.org/http://dx.doi.org/10.1016/S0016-7037(99)00270-7

Lodeiro, P., Rey-Castro, C., David, C., Achterberg, E.P., Puy, J., Gledhill, M., 2020. Acid-base properties of dissolved organic matter extracted from the marine environment. Sci. Total Environ. 729, 138437. https://doi.org/10.1016/j.scitotenv.2020.138437

Lønborg, C., Carreira, C., Jickells, T., Álvarez-Salgado, X.A., 2020. Impacts of global change on ocean dissolved organic carbon (DOC) cycling. Front. Mar. Sci. 7, 466.

https://doi.org/10.3389/fmars.2020.00466
Marsay, C.M., Barrett, P.M., McGillicuddy, D.J., Sedwick, P.N., 2017. Distributions, sources, and transformations of dissolved and particulate iron on the Ross Sea continental shelf during summer. J. Geophys. Res. Ocean. 122, 6371–6393. https://doi.org/10.1002/2017JC013068
Mawji, E., Gledhill, M., Milton, J.A.J.A., Zubkov, M.V.M. V, Thompson, A., Wolff, G.A.G.A., Achterberg, E.P.E.P., 2011. Production of siderophore type chelates in Atlantic Ocean waters enriched with different carbon and nitrogen sources. Mar. Chem. 124, 90–99. https://doi.org/10.1016/j.marchem.2010.12.005
Meeussen, J.C.L., 2003. Orchestra: An object-oriented framework for implementing chemical equilibrium models. Environ. Sci. Technol. 37, 1175–1182. https://doi.org/10.1021/es025597s
Mehrbach, C., Culberson, C.H., Hawley, J.E., Pytkowicz, R.M., 1973. Measurement of the apparent dissociation constants of carbonic acid in seawater at atmospheric pressure. Limnol. Oceanogr. 18, 897–906.
Millero, F.J., Woosley, R., Ditrolio, B., Waters, J., 2009. Effect of ocean acidification on the speciation of metals in seawater. Oceanography 22, 72–85.
Milne, C.J., Kinniburgh, D.G., Tipping, E., 2001. Generic NICA-Donnan model parameters for proton binding by humic substances. Environ. Sci. Technol. 35, 2049–2059. https://doi.org/10.1021/es000123j
Milne, C.J., Kinniburgh, D.G., van Riemsdijk, W.H., Tipping, E., 2003. Generic NICA−Donnan model parameters for metal-ion binding by humic substances. Environ. Sci. Technol. 37, 958–971. https://doi.org/10.1021/es0258879
Muller-Karger, F.E., Varela, R., Thunell, R., Luerssen, R., Hu, C., Walsh, J.J., 2005. The importance of continental margins in the global carbon cycle. Geophys. Res. Lett. 32, 1–4. https://doi.org/10.1029/2004GL021346
Muller, F.L.L., 2018. Exploring the potential role of terrestrially derived humic substances in the marine biogeochemistry of iron. Front. Earth Sci. 6, 1–20. https://doi.org/10.3389/feart.2018.00159
Ndungu, K., 2012. Model predictions of copper speciation in coastal water compared to measurements by analytical voltammetry. Environ. Sci. Technol. 46, 7644–7652. https://doi.org/10.1021/es301017x
Nedelec, F., Statham, P.J., Mowlem, M., 2007. Processes influencing dissolved iron distributions below the surface at the Atlantic Ocean-Celtic Sea shelf edge. Mar. Chem. 104, 156–170.

https://doi.org/10.1016/j.marchem.2006.10.011
Nimmo, M., van den Berg, C.M.G., Brown, J., 1989. The Chemical speciation of dissolved nickel, copper, vanadium and iron in Liverpool Bay, Irish Sea. Estuar. Coast. Shelf Sci. 29, 57–74.
Obata, H., Karatani, H., Nakayama, E., 1993. Automated-determination of iron in seawater by chelating resin concentration and chemiluminescence detection. Anal. Chem. 65, 1524–1528.
Pierrot, D., Lewis, E., Wallace, D.W.R., 2006. MS Excel program developed for CO_2 system calculations. ORNL/CDIAC-105a. Carbon Dioxide Inf. Anal. Center, Oak Ridge Natl. Lab. US Dep. Energy, Oak Ridge, Tennessee.
Pinheiro, J.P., Rotureau, E., Duval, J.F.L., 2021. Addressing the electrostatic component of protons binding to aquatic nanoparticles beyond the Non-Ideal Competitive Adsorption (NICA)-Donnan level: Theory and application to analysis of proton titration data for humic matter. J. Colloid Interface Sci. 583, 642–651. https://doi.org/10.1016/j.jcis.2020.09.059
Pižeta, I., Sander, S.G., Hudson, R.J.M., Omanović, D., Baars, O., Barbeau, K.A., Buck, K.N., Bundy, R.M., Carrasco, G., Croot, P.L., Garnier, C., Gerringa, L.J.A., Gledhill, M., Hirose, K., Kondo, Y., Laglera, L.M., Nuester, J., Rijkenberg, M.J.A., Takeda, S., Twining, B.S., Wells, M., 2015. Interpretation of complexometric titration data: An intercomparison of methods for estimating models of trace metal complexation by natural organic ligands. Mar. Chem. 173, 3–24. https://doi.org/http://dx.doi.org/10.1016/j.marchem.2015.03.006
Poorvin, L., Sander, S.G., Velasquez, I., Ibisanmi, E., LeCleir, G.R., Wilhelm, S.W., 2011. A comparison of Fe bioavailability and binding of a catecholate siderophore with virus-mediated lysates from the marine bacterium Vibrio alginolyticus PWH3a. J. Exp. Mar. Bio. Ecol. 399, 43–47. https://doi.org/10.1016/j.jembe.2011.01.016
Ringbom, A., Still, E., 1972. The calculation and use of a coefficients. Anal. Chim. Acta 59, 143–146.
Rose, A.L., Waite, T.D., 2005. Reduction of organically complexed ferric iron by superoxide in a simulated natural water. Environ. Sci. Technol. 39, 2645–2650. https://doi.org/10.1021/es048765k
Rusiecka, D., Gledhill, M., Milne, A., Achterberg, E.P., Annett, A.L., Atkinson, S., Birchill, A., Karstensen, J., Lohan, M., Mariez, C., Middag, R., Rolison, J.M., Tanhua, T., Ussher, S., Connelly, D., 2018. Anthropogenic Signatures of Lead in the Northeast Atlantic. Geophys. Res. Lett. 45, 2734–2743. https://doi.org/10.1002/2017GL076825
Sander, S.G., Hunter, K.A., Harms, H., Wells, M., 2011. Numerical approach to speciation and

estimation of parameters used in modeling trace metal bioavailability. Environ. Sci. Technol. 45, 6388–6395. https://doi.org/10.1021/es200113v

Schlitzer, R., 2015. Ocean Data View, odv. awi. de.

Schlosser, C., Streu, P., Frank, M., Lavik, G., Croot, P.L., Dengler, M., Achterberg, E.P., 2018. H2S events in the Peruvian oxygen minimum zone facilitate enhanced dissolved Fe concentrations. Sci. Rep. 8, 12642. https://doi.org/10.1038/s41598-018-30580-w

Shaked, Y., Lis, H., 2012. Disassembling iron availability to phytoplankton. Front. Microbiol. 3, 123. https://doi.org/10.3389/fmicb.2012.00123

Shi, D., Xu, Y., Hopkinson, B.M., Morel, F.M.M., 2010. Effect of ocean acidification on iron availability to marine phytoplankton. Science (80-.). 327, 676–679. https://doi.org/10.1126/science.1183517

Slagter, H.A., Laglera, L.M., Sukekava, C., Gerringa, L.J.A., 2019. Fe-Binding Organic Ligands in the Humic-Rich TransPolar Drift in the Surface Arctic Ocean Using Multiple Voltammetric Methods. J. Geophys. Res. Ocean. 124, 1491–1508. https://doi.org/10.1029/2018JC014576

Smith, R.M., Martell, A.E., Motekaitis, R.J., 2004. NIST critically selected stability constants of metal complexes database. NIST Stand. Ref. Database 46 National Institute of Standard and Technology, Gai.

Stockdale, A., Tipping, E., Hamilton-Taylor, J., Lofts, S., 2011. Trace metals in the open oceans: Speciation modelling based on humic-type ligands. Environ. Chem. 8, 304–319. https://doi.org/10.1071/EN11004

Stockdale, A., Tipping, E., Lofts, S., 2015. Dissolved trace metal speciation in estuarine and coastal waters: Comparison of WHAM/Model VII predictions with analytical results. Environ. Toxicol. Chem. 34, 53–63. https://doi.org/10.1002/etc.2789

Stockdale, A., Tipping, E., Lofts, S., Mortimer, R.J.G., 2016. Effect of Ocean Acidification on Organic and Inorganic Speciation of Trace Metals. Environ. Sci. Technol. 50, 1906–1913. https://doi.org/10.1021/acs.est.5b05624

Sukekava, C., Downes, J., Slagter, H.A., Gerringa, L.J.A., Laglera, L.M., 2018. Determination of the contribution of humic substances to iron complexation in seawater by catalytic cathodic stripping voltammetry. Talanta 189, 359–364. https://doi.org/10.1016/J.TALANTA.2018.07.021

Sunda, W.G., Huntsman, S.A., 1995. Iron uptake and growth limitation in oceanic and coastal phytoplankton. Mar. Chem. 50, 189–206. https://doi.org/10.1016/0304-4203(95)00035-P

Tagliabue, A., Aumont, O., Death, R., Dunne, J.P., Dutkiewicz, S., Galbraith, E., Misumi, K., Moore,

J.K., Ridgwell, A., Sherman, E., Stock, C., Vichi, M., Völker, C., Yool, A., 2016. How well do global ocean biogeochemistry models simulate dissolved iron distributions? Global Biogeochem. Cycles 30, 149–174. https://doi.org/10.1002/2015GB005289

Tagliabue, A., Williams, R.G., Rogan, N., Achterberg, E.P., Boyd, P.W., 2014. A ventilation-based framework to explain the regeneration-scavenging balance of iron in the ocean. Geophys. Res. Lett. 41, 7227–7236. https://doi.org/10.1002/2014GL061066

Timmermans, K.R., van der Wagt, B., Veldhuis, M.J.W., Maatman, A., de Baar, H.J.W., 2005. Physiological responses of three species of marine pico-phytoplankton to ammonium, phosphate, iron and light limitation. J. Sea Res. 53, 109–120.

Tipping, E., Lofts, S., Sonke, J.E., 2011. Humic Ion-Binding Model VII: a revised parameterisation of cation-binding by humic substances. Environ. Chem. 8, 225–235. https://doi.org/http://dx.doi.org/10.1071/EN11016

Tipping, E., Lofts, S., Stockdale, A., 2016. Metal speciation from stream to open ocean: Modelling v. measurement. Environ. Chem. 13, 464–477. https://doi.org/10.1071/EN15111

Town, R.M., Filella, M., 2000. Dispelling the myths: Is the existence of L1 and L2 ligands necessary to explain metal ion speciation in natural waters? Limnol. Oceanogr. 45, 1341–1357.

Town, R.M., Van Leeuwen, H.P., 2005. Measuring marine iron(III) complexes by CLE-AdSV. Environ. Chem. 2, 80–84.

Turner, D.R., Achterberg, E.P., Chen, C.-T.A., Clegg, S.L., Hatje, V., Maldonado, M.T., Sander, S.G., van den Berg, C.M.G., Wells, M., 2016. Toward a quality-controlled and accessible Pitzer model for seawater and related systems. Front. Mar. Sci. 3, 139. https://doi.org/10.3389/fmars.2016.00139

Uppström, L.R., 1974. The boron/chlorinity ratio of deep-sea water from the Pacific Ocean. Deep Sea Res. Oceanogr. Abstr. 21, 161–162. https://doi.org/http://dx.doi.org/10.1016/0011-7471(74)90074-6

Ussher, S.J., Worsfold, P.J., Achterberg, E.P., Laës, A., Blain, S., Laan, P., De Baar, H.J.W., 2007. Distribution and redox speciation of dissolved iron on the European continental margin. Limnol. Oceanogr. 52, 2530–2539. https://doi.org/10.4319/lo.2007.52.6.2530

van den Berg, C.M.G., 1995. Evidence for organic complexation of iron in seawater. Mar. Chem. 50, 139–157. https://doi.org/10.1016/0304-4203(95)00032-M

van den Berg, C.M.G., 1991. Potentials and potentialities of cathodic stripping voltammetry of trace elements in natural waters. Anal. Chim. Acta 250, 165–276.

Van Leeuwen, H.P., Town, R.M., 2005. Kinetic limitations in measuring stabilities of metal complexes by competitive ligand exchange-adsorptive stripping voltammetry (CLE-AdSV). Environ. Sci. Technol. 39, 7217–7225. https://doi.org/10.1021/es050367+

Voelker, B.M., Kogut, M.B., 2001. Interpretation of metal speciation data in coastal waters: the effects of humic substances on copper binding as a test case. Mar. Chem. 74, 303–318. https://doi.org/http://dx.doi.org/10.1016/S0304-4203(01)00022-6

Vraspir, J.M., Butler, A., 2009. Chemistry of Marine Ligands and Siderophores. Ann. Rev. Mar. Sci. 1, 43–63.

Waska, H., Koschinsky, A., Dittmar, T., 2016. Fe- and Cu-complex formation with artificial ligands investigated by ultra-high resolution Fourier-transform ion cyclotron resonance mass Spectrometry (FT-ICR-MS): Implications for natural metal-organic complex studies. Front. Mar. Sci. 3, 119. https://doi.org/10.3389/fmars.2016.00119

Worsfold, P.J., Achterberg, E.P., Birchill, A.J., Clough, R., Leito, I., Lohan, M.C., Milne, A., Ussher, S.J., 2019. Estimating uncertainties in oceanographic trace element measurements. Front. Mar. Sci. 6, 1–9. https://doi.org/10.3389/fmars.2018.00515

Wu, J., Luther III, G.W., 1995. Complexation of iron(III) by natural organic ligands in the Northwest Atlantic Ocean by a competitive ligand equilibration method and a kinetic approach. Mar. Chem. 50, 159–179.

Wu, J., Luther III, G.W., 1994. Size-fractionated iron concentrations in the water column of the western North Atlantic Ocean. Limnol. Oceanogr. 39, 1119–1129. https://doi.org/10.4319/lo.1994.39.5.1119

Ye, Y., Völker, C., Gledhill, M., 2020. Exploring the Iron-Binding Potential of the Ocean Using a Combined pH and DOC Parameterization. Global Biogeochem. Cycles 34, 1–16. https://doi.org/10.1029/2019GB006425

Zhang, J., Kattner, G., Koch, B.P., 2019. Interactions of trace elements and organic ligands in seawater and implications for quantifying biogeochemical dynamics: A review. Earth-Science Rev. 192, 631–649. https://doi.org/10.1016/j.earscirev.2019.03.007

Zhu, K., Hopwood, M.J., Groenenberg, J.E., Engel, A., Achterberg, E.P., Gledhill, M., 2021. Influence of pH and dissolved organic matter on iron speciation and apparent iron solubility in the Peruvian shelf and slope region. Enviromental Sci. Technol. Accepted.

Abbreviations

Terms	Description
$k^{cond}_{FeNN3,Fe',or\ Fe3+}$	Conditional stability constants describing the strength of a complex $FeNN_3$ relative to inorganic Fe concentration or free Fe^{3+} concentrations
$\alpha_{FeNN3,Fe',or\ Fe3+}$	Side reaction coefficient for $FeNN_3$ expressed relative to inorganic Fe concentration or free Fe^{3+} concentrations
$k^{cond}_{FeNN3,H+}$	Stability constants of HNN used in an ion pairing model, that would account for competition between NN^-, H^+, Fe^{3+} and OH^- at the ionic strengths and pH relevant to our study
Detection window	The detection window describes the range over which competition between NN^- and binding sites (L^-) can be detected. It is traditionally defined as ± 1 or 1.5 log units of $\alpha_{FeNN3,Fe'}$ (Apte et al., 1988)
$k^{cond}_{FeL,Fe'}$	Conditional stability constants describing the strength of a complex FeL relative to inorganic Fe concentration
$a_{FeL,Fe'}$	Side reaction coefficient for metal-natural ligand expressed relative to inorganic Fe concentration
$logK_{Fe(III)1\ or\ 2}$	The median value of distribution of binding affinity of Fe(III) binding to organic matter in the NICA-Donnan model
$n_{Fe(III)1\ or\ 2}$	The non-ideal constants describe the ratio of Fe(III) to binding sites
$[Fe^{3+}]_{titration}$	Free Fe concentrations determined in titrations
$[Fe^{3+}]_{cal}$	Free Fe concentrations calculated using an ion pairing model in the absence of organic matter
$[Fe^{3+}]_{NICA}$	Free Fe concentrations calculated using the NICA-Donnan model in the presence of organic matter
$DFe^*_{titration}$	The non-labile fraction of Fe determined in titrations (i.e. total Fe – $FeNN_3$)
DFe^*_{NICA}	The non-labile fraction of Fe calculated using the NICA-Donnan model in the presence of organic matter (i.e. total Fe – $FeNN_3$)

1388